

AD-A160 434

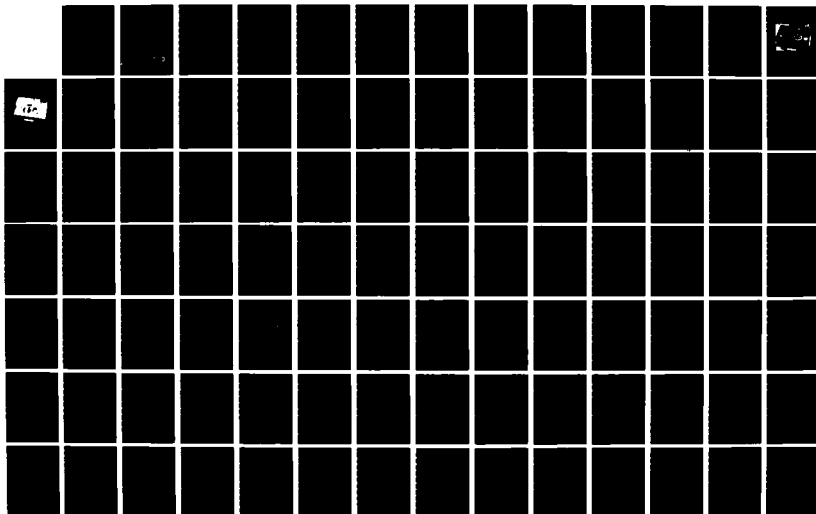
FLIGHT MODEL DISCHARGE SYSTEM(U) HUGHES RESEARCH LABS
MALIBU CA R R ROBSON ET AL. MAR 85 SCIENTIFIC-1
AFGL-TR-85-0044 F19628-03-C-0143

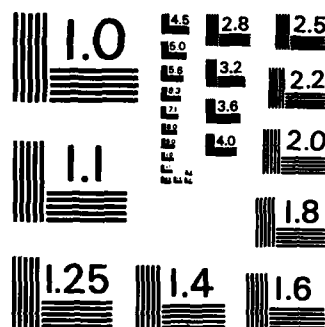
1/2

UNCLASSIFIED

F/G 20/3

NL





MICROCOPY RESOLUTION TEST CHART
NATIONAL BUREAU OF STANDARDS-1963-A

AD-A160 434

13

AFGL-TR-85-0044

FLIGHT MODEL DISCHARGE SYSTEM

R. R. Robson
W. S. Williamson

Hughes Research Laboratories
3011 Malibu Canyon Road
Malibu, CA 90265

Scientific Report No. 1

March 1985

Approved for public release; distribution unlimited.

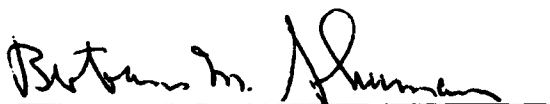
Air Force Geophysics Laboratory
Air Force Systems Command
United States Air Force
Hanscom AFB, MA 01731

DTIC
ELECTE
OCT 22 1985
S
E
D

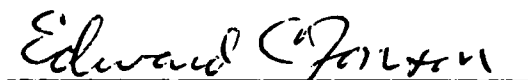
85 10 22 029

DTIC FILE COPY

"This technical report has been reviewed and is approved for publication"




BERTRAM M. SHUMAN
Contract Manager



EDWARD JONSON, LtCol, USAF, Chief
Space Systems Technology Branch

FOR THE COMMANDER


RITA C. SAGALYN, Director
Space Physics Division

This report has been reviewed by the ESD Public Affairs Office (PA) and is releasable to the National Technical Information Service (NTIS).

Qualified requestors may obtain additional copies from the Defense Technical Information Center. All others should apply to the National Technical Information Service.

If your address has changed, or if you wish to be removed from the mailing list, or if the addressee is no longer employed by your organization, please notify AFGL/DAA, Hanscom AFB, MA 01731. This will assist us in maintaining a current mailing list.

UNCLASSIFIED

SECURITY CLASSIFICATION OF THIS PAGE

AD - A160434

REPORT DOCUMENTATION PAGE

1a. REPORT SECURITY CLASSIFICATION Unclassified			1b. RESTRICTIVE MARKINGS		
2a. SECURITY CLASSIFICATION AUTHORITY			3. DISTRIBUTION/AVAILABILITY OF REPORT Approved for public release; distribution unlimited.		
2b. DECLASSIFICATION/DOWNGRADING SCHEDULE					
4. PERFORMING ORGANIZATION REPORT NUMBER(S)			5. MONITORING ORGANIZATION REPORT NUMBER(S) AFGL-TR-85-0044		
6a. NAME OF PERFORMING ORGANIZATION Hughes Research Laboratories		6b. OFFICE SYMBOL (If applicable)	7a. NAME OF MONITORING ORGANIZATION Air Force Geophysics Laboratory		
6c. ADDRESS (City, State and ZIP Code) 3011 Malibu Canyon Rd. Malibu, CA 90265			7b. ADDRESS (City, State and ZIP Code) Hanscom AFB Massachusetts 01731		
8a. NAME OF FUNDING/SPONSORING ORGANIZATION Air Force Geophysics Lab.		8b. OFFICE SYMBOL (If applicable) AFGL/PHK	9. PROCUREMENT INSTRUMENT IDENTIFICATION NUMBER F19628-83-C-0143		
8c. ADDRESS (City, State and ZIP Code) Hanscom AFB Massachusetts 01731			10. SOURCE OF FUNDING NOS.		
			PROGRAM ELEMENT NO. 63410F	PROJECT NO. 2823	TASK NO. 01
					WORK UNIT NO. AA
11. TITLE (Include Security Classification) Flight Model Discharge System					
12. PERSONAL AUTHOR(S) R.R. Robson, W.S. Williamson					
13a. TYPE OF REPORT Scientific Report No. 1		13b. TIME COVERED FROM 9/83 TO 10/84		14. DATE OF REPORT (Yr., Mo., Day) March 1985	
15. PAGE COUNT 100					
16. SUPPLEMENTARY NOTATION					
17. COSATI CODES			18. SUBJECT TERMS (Continue on reverse if necessary and identify by block number)		
FIELD	GROUP	SUB. GR.	Spacecraft Charging; FMDS, Flight Model Discharge System, Spacecraft Automatic Active Discharge System, A		
19. ABSTRACT (Continue on reverse if necessary and identify by block number) A breadboard design for a Flight Model Discharge System (FMDS) to prevent charging of spacecraft in geosynchronous orbit has been performed. Operational characteristics of the entire system are presented, including the electrostatic analyzer, surface potential monitor, transient pulse monitor, plasma source, and microprocessor-based controller. Design considerations that led to the final system configuration are also presented. K. ...					
20. DISTRIBUTION/AVAILABILITY OF ABSTRACT UNCLASSIFIED/UNLIMITED <input checked="" type="checkbox"/> SAME AS RPT. <input type="checkbox"/> DTIC USERS <input type="checkbox"/>			21. ABSTRACT SECURITY CLASSIFICATION Unclassified		
22a. NAME OF RESPONSIBLE INDIVIDUAL Bert Shuman			22b. TELEPHONE NUMBER (Include Area Code) 616-861-3991		22c. OFFICE SYMBOL AFGL/PHK

TABLE OF CONTENTS

SECTION		PAGE
1	INTRODUCTION.....	7
2	FMDS TOTAL SYSTEM.....	9
	2.1 Overall System.....	11
	2.2 Components.....	14
3	PLASMA SOURCE.....	25
	3.1 Plasma Generator.....	25
	3.2 Expellant Storage and Control System.....	25
	3.3 Plasma Generator Electronics Design.....	30
4	ELECTROSTATIC ANALYZERS.....	39
	4.1 Cylindrical-ESA Operating Principles.....	39
	4.2 ESA Design.....	42
5	SURFACE POTENTIAL MONITORS.....	55
	5.1 Design Philosophy for the SPM Sensor Head.....	56
	5.2 SPM Electronics Design.....	61
6	TRANSIENT PULSE MONITOR.....	65
	6.1 Selection of Detection Methods.....	66
	6.2 TPM System Design.....	68
7	CONTROLLER.....	73
	7.1 Controller Hardware Design.....	73
	7.2 Controller Software Design.....	76
8	SYSTEM DESIGN.....	87
	8.1 Electrical Design.....	89
	8.2 Commands and Telemetry.....	89
9	CONCLUSION.....	95
	REFERENCES.....	97

LIST OF ILLUSTRATIONS

FIGURE		PAGE
2-1	Block diagram of the Flight Model Discharge System.....	10
2-2	Model of the FMDS with its cover in place.....	12
2-3	Model of the FMDS with its cover removed.....	13
2-4	Shift in the observed ion and electron spectra caused by environmental conditions conducive to charging and by actual charging of the spacecraft.....	16
2-5	Charging characteristics of a shaded dielectric sensor.....	17
3-1	Simple schematic of the xenon plasma source...	27
3-2	Design of the expellant feed system.....	28
3-3	Plasma generator electronics block diagram.....	31
3-4	Simplified schematic of a half-wave flyback inverter.....	34
3-5	Bipolar log electrometer schematic.....	37
4-1	ESA operating principles.....	40
4-2	Basic design of the electrostatic analyzer detection assembly.....	45
4-3	General physical design of the entire ESA package.....	47
4-4	Basic design of the ESA electronics for the ion detection head.....	48
4-5	Electronic design of the ESA plate voltage sweep control.....	50
5-1	NASA surface voltage sensor head detail.....	57
5-2	Schematic cross section of Hughes SPM sensor head redesign.....	59
5-3	Surface potential monitor functional diagram..	62

FIGURE		PAGE
6-1	Block diagram of the TPM.....	69
6-2	TPM sensing head design.....	70
7-1	Controller hardware block diagram.....	74
7-2	Controller executive routine.....	77
7-3	Charging detection algorithm.....	80
7-4	Template-matching algorithm.....	83
7-5	Spiegel's distribution-function algorithm.....	85
8-1	Ground return isolation.....	90
8-2	28-V power isolation regulator block diagram..	91
8-3	Typical optical isolation and driver circuits.....	93

LIST OF TABLES

TABLE		PAGE
2-1	Electrostatic Analyzer Specifications and Breadboard Design.....	19
2-2	Surface Potential Monitor Specifications and Breadboard Design.....	20
2-3	Transient Pulse Monitor Specification and Breadboard Design.....	21
2-4	Plasma Source Specifications and Breadboard Design.....	22
2-5	Controller Specifications and Breadboard Design.....	23
3-1	SPACECLAMP Plasma Generator Characteristics...	26
3-2	Dc-to-dc Converter Characteristic Comparison..	33
4-1	Basic Specification for the ESA Design.....	43
4-2	Energy Detection Characteristics of ESA.....	44
4-3	ESA Commands Format.....	51
4-4	ESA Data Format.....	52
8-1	Estimated Response Times of the FMDS for the Various Charging Sensors.....	88

Accession For	
NTIS GRA&I	<input checked="" type="checkbox"/>
DTIC TAB	<input type="checkbox"/>
Unannounced	<input type="checkbox"/>
Justification	
By	
Distribution/	
Availability Codes	
Dist	Avail and/or Special
A-1	



SECTION 1

INTRODUCTION

The objectives of the FMDS program are the design, development, fabrication, test and delivery of two flight units of a satellite Flight Model Discharge System (FMDS). The FMDS is a stand-alone system capable of autonomous operation (except for power) that will monitor spacecraft potential, determine when spacecraft charging is present, and operate a discharge device to eliminate potentials and maintain the spacecraft in a neutral charge state. The FMDS is designed to be incorporated into the "housekeeping" function of any spacecraft which may be subject to spacecraft charging. While full ground-command capability is retained for redundancy, only a "power on" command is required to activate the system. In addition to the capability for ground or remote command override of its autonomous operation, the FMDS also provides telemetry signals to monitor such functions as sensor outputs, controller "commands", plasma source operation, gas supply in the reservoir tank, and system state-of-health diagnostics (i.e., temperature, voltages, and currents).

The technical discussion which follows presents the results of the first year's effort on the FMDS contractual program which is being carried out by Hughes Research Laboratories in Malibu, CA. An overview of Hughes' breadboard design is presented, followed by an in-depth treatment of the FMDS components.

SECTION 2

FMDS TOTAL SYSTEM

The FMDS is a stand-alone system capable of autonomous operation (except for power) that monitors vehicle potential, determines when spacecraft charging is present, and operates a discharge device to eliminate potential build-up and maintain the vehicle in a neutral charge state. The FMDS is designed to be incorporated into the "housekeeping" functions of any vehicle which may develop spacecraft charging. While full ground-command capability is retained for redundancy, only a "power on" command is required to activate the system. It detects charging, operates to neutralize the charging, and returns to the passive mode when the charging hazard is no longer present.

The FMDS consists of three types of components:

- o Charging sensors:
 - (1) Electrostatic Analyzers. These sensors detect absolute charging relative to the ambient plasma in space.
 - (2) Surface Potential Monitors. These sensors determine differential charging relative to spacecraft ground.
 - (3) Transient Pulse Monitor. This sensor detects the electromagnetic pulses generated by the onset of arcing.
- o An active discharge device (plasma source).
- o A control unit to interpret the sensor outputs, determine when and if charging is occurring, and control the discharge device.

A block diagram of the system is shown in Figure 2-1.

The controller incorporates comprehensive charging-detection algorithms which contain ground-alterable parameters to allow in-space refinement of FMDS operation. The controller incorporates redundant components and fault-tolerant software to permit the FMDS to continue operation in the face of specific faults or failures. In addition it has the capability for ground or

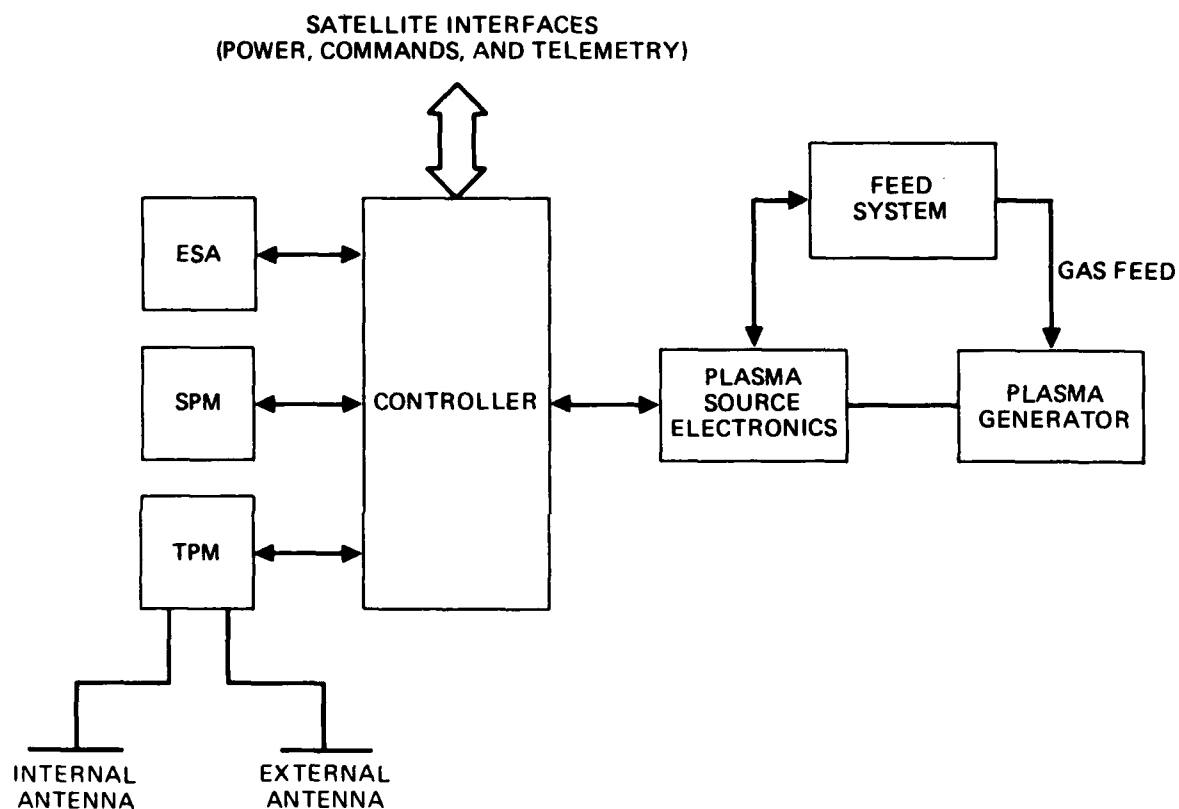


Figure 2-1. Block diagram of the Flight Model Discharge System (FMDS).

remote-command override of its autonomous operation, and also provides telemetry signals to monitor such functions as sensor outputs, controller status flags, plasma source operation, gas supply pressure in the reservoir tank, temperature, voltages, currents, etc.

The FMDS is ultimately intended for extended satellite operation at geosynchronous orbit, but its earliest flight may be aboard the Space Shuttle. Therefore, it is designed to withstand the launch and operating environments of both these regimes. Emphasis is placed on safety and reliability, with consideration given toward low operating and transient voltages.

2.1 OVERALL SYSTEM

Hughes' conceptual FMDS configuration is shown in Figures 2-2 and 2-3. All components of the system are attached to a common honeycomb-structure mounting plate to provide a simple, lightweight and structurally sturdy interface with the host spacecraft. No attempt is made in this model to indicate the exact interface of the FMDS with the host spacecraft since Hughes has no way of knowing at this time what platform will be provided. In fact, because of this uncertainty, Hughes has elected to design the FMDS so that it functions independently of the characteristics of the host vehicle. The structurally integrated design approach will also facilitate system testing in both laboratory vacuum chambers and environmental test fixtures (vibration, thermal/vacuum, etc.).

Because of the diversity of functions required of the various FMDS components, each element is packaged separately and attached separately to the common mounting plate. Maintaining separation between each of the components has the added advantage of facilitating later substitutions of upgraded component designs if such upgrades become available in the future.

The two Surface Potential Monitors (SPMs) and the ion and electron Electrostatic Analyzers (ESAs) are mounted on one end of the FMDS mounting plate to provide both maximal and similar

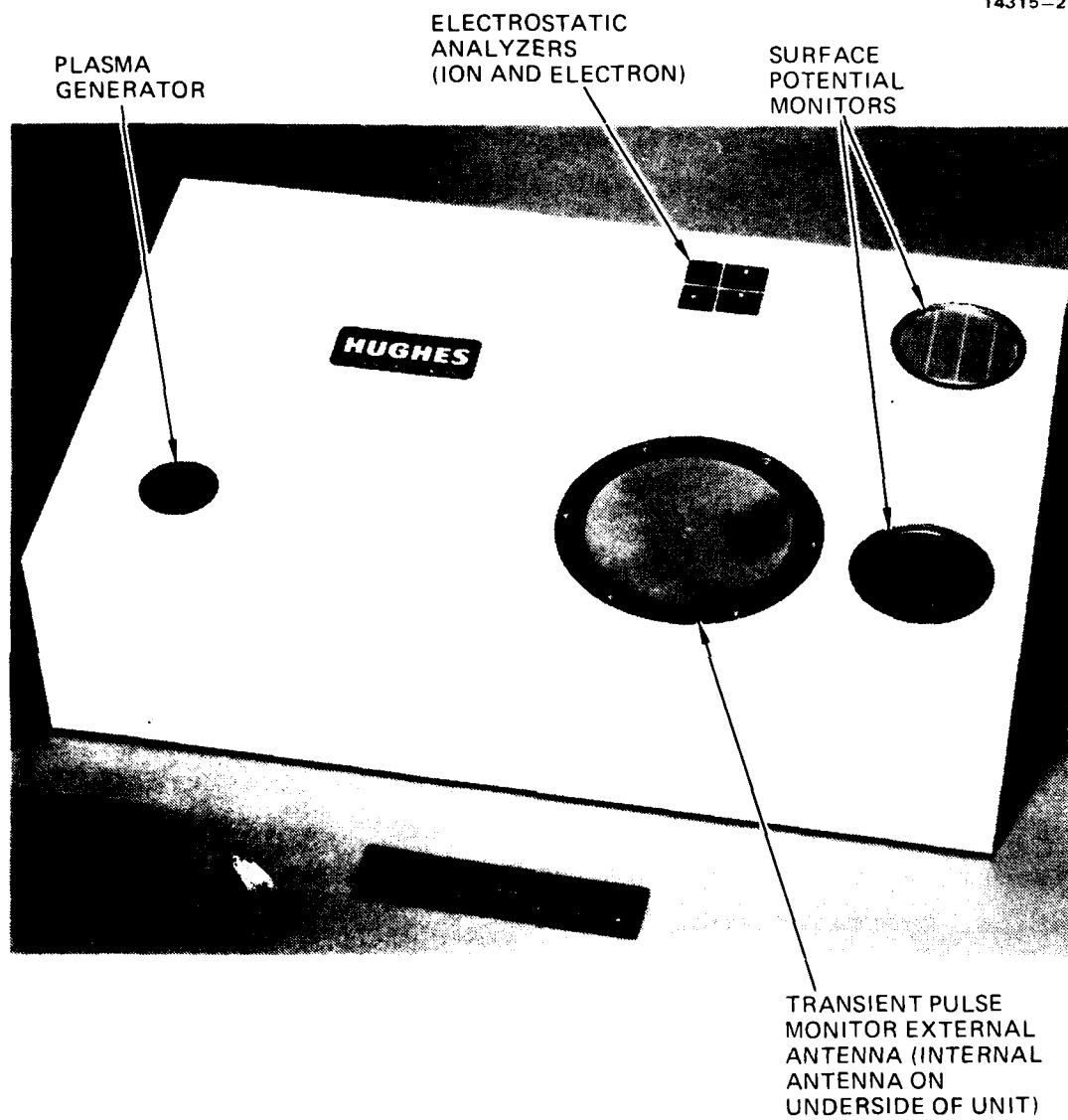


Figure 2-2. Model of the FMDS with its cover in place.

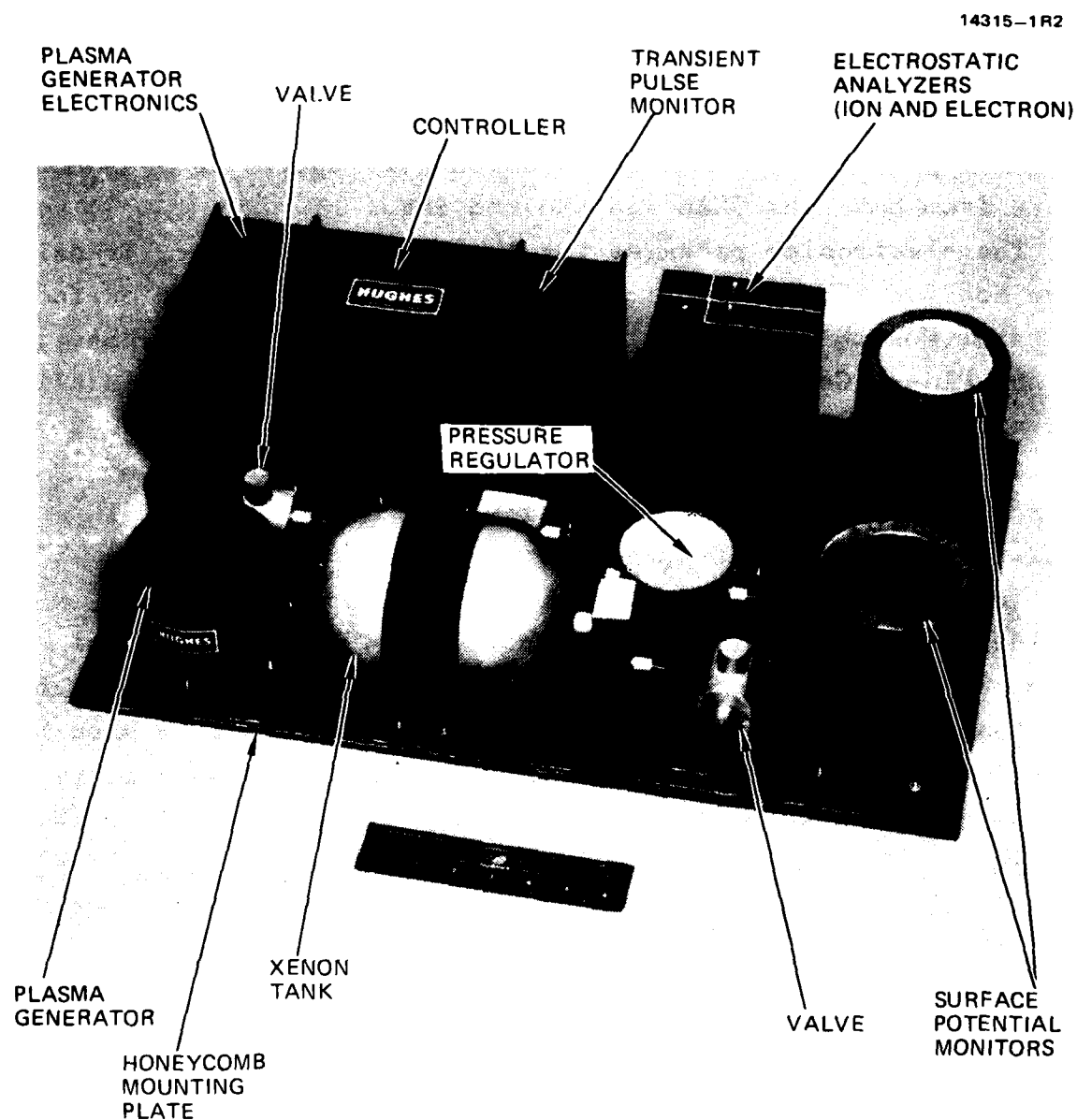


Figure 2-3. Model of the FMDS with its cover removed.

exposure of the sensors to incoming particle flux while avoiding (as much as possible) any local distortions of electrostatic equipotentials which might be caused by other devices such as the Plasma Source or Transient Pulse Monitor.

The Plasma Source is located at the other end of the FMDS where it is furthest from the charged-particle entrance apertures of the ESAs; this will minimize the introduction of plasm-source-generated particles. In this location, the source is reasonably remote from both the ESAs and the two SPMs.

The electronics packages for the Plasma-Generator, Transient Pulse Monitor (TPM), and Microprocessor Controller; the Surface Potential Monitors (SPMs); the Electrostatic Analyzers (ESAs); and the Plasma Generator are all at the same height. This allows a cover to be added to the FMDS to form a ground plane and to provide a mounting surface for the Transient Pulse Monitor external antenna. Thermal control surfaces and/or thermal blankets can also be attached to this cover.

Inasmuch as the FMDS is intended for satellite use, considerations of minimizing weight, volume and power are of utmost concern. The overall FMDS system is expected to weight less than 11.4 kg (25 lbs.), and consume less than 10 W when the plasma source is not activated, and less than 22 W when it is activated. The overall dimensions are 16.5 x 38.1 x 61 cm (6.5 x 15 x 24 in).

2.2 COMPONENTS

The Electrostatic Analyzers (ESAs) will look at the energy distribution (from 0 to 20 keV) of the particles incident upon the satellite. There will be a shift in this energy distribution when the environmental conditions are conducive to spacecraft charging (caused by a change in the environmental conditions), and another shift directly related to the potential of the satellite frame relative to the space potential. Since the ESAs are referenced to the satellite frame and the particles originate at space potential, any change in the potential of the satellite

frame will appear as a change in the particle energy distributions. Algorithms in the controller will detect the shift in the particle energy distributions (Figure 2-4) in order to (1) provide an early warning that the environmental conditions are conducive to spacecraft charging (by detection of electrons) and (2) detect that charging of the satellite frame has exceeded a threshold level (by proton detection) and provide a signal to turn on the Plasma Source.

The Surface Potential Monitor will detect the onset of differential charging of the satellite dielectric surfaces. When the satellite is in sunlight and charging conditions exist, the isolated dielectric surfaces that are shaded will charge much faster than the satellite frame because of the lack of photo-emission from these shaded surfaces (Figure 2-5). Therefore, by measuring the potential on the surface of a shaded dielectric sensor, differential charging can be detected quickly and prior to the detection of satellite frame charging by the ESA. When the satellite is in eclipse, however, satellite-frame charging occurs faster than differential charging (Figure 2-5). In this circumstance the ESA will be the prime detector.

The Transient Pulse Monitor (TPM) will detect electrical discharges that occur on the surface of the satellite due to differential charging. A floating-plate sensor is employed to pick up radiated electric fields caused by these discharges. If electrical discharges are occurring, it implies that the satellite is charged up, that the Plasma Generator should be turned on, and that the other sensors have failed to detect the charging. The TPM has ground-adjustable parameters and can be commanded to ignore transients which occur within one second following receipt of a command by the spacecraft. Its capabilities are designed to avoid false arc-discharging alarms.

The Plasma Generator emits xenon ions and electrons in sufficient quantity (>1 ma) to bathe the satellite in a conductive low energy (<50 eV) plasma. This conductive plasma will drain the charge from dielectric surfaces and also form a "plasma

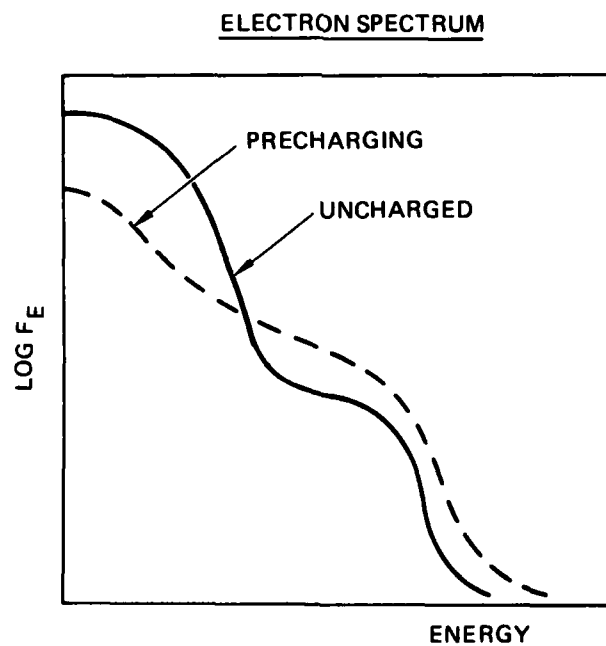
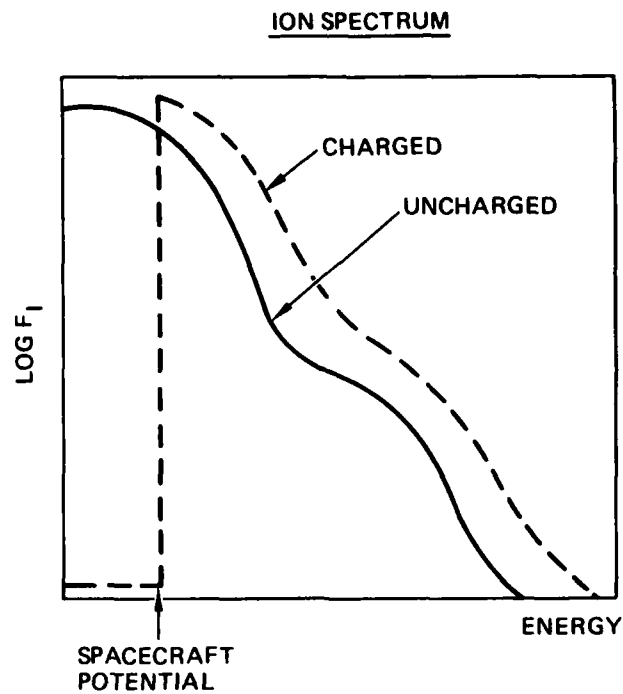


Figure 2-4. Shift in the observed ion and electron spectra caused by environmental conditions conducive to charging and by actual charging of the spacecraft.

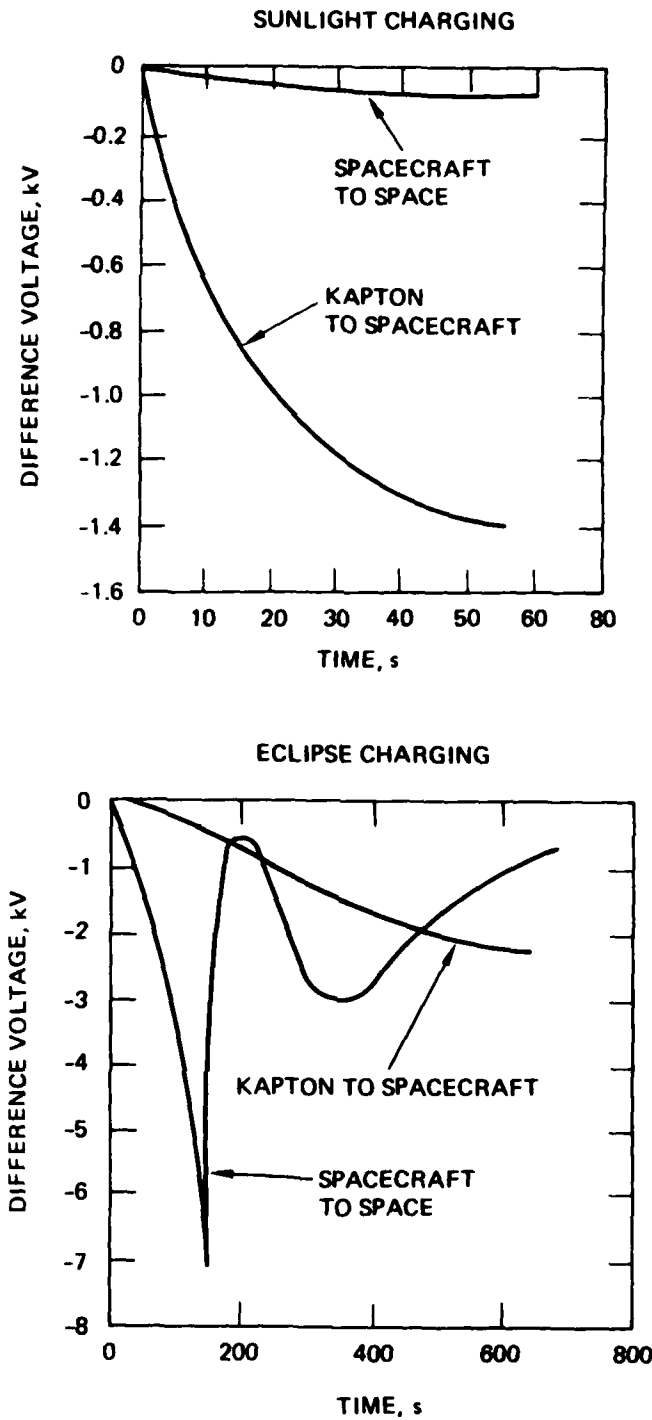


Figure 2-5.
Charging characteristics of a shaded
dielectric sensor.

bridge" to the surrounding natural space-plasma environment. The Plasma Generator is capable of igniting in less than one second (<1 s), operating for 1200 hours, and executing 1000 on/off cycles. It requires three power supplies and a gas feed system consisting of a xenon storage tank, pressure regulator, valves and flow regulator.

The Controller provides for autonomous control of the FMDS relative to the remainder of the satellite. It is also the device which ties the other units of the FMDS together. The brain of the controller is a microprocessor which contains the algorithms necessary to interpret the data from the sensors and command the Plasma Generator to turn on when spacecraft charging is occurring and then turn off when it is no longer required. The Plasma Generator is turned OFF after either a programmable time-out, when the emission current from the Plasma Generator has been less than a threshold value for a period of time, and/or the ambient electron environment returns to a quiescent condition. The Controller also provides the command and telemetry interface with the satellite.

Tables 2-1 through 2-5 list the major contractual specifications for the ESAs, SPMs, TPM, Plasma Source, and Controller, respectively. The respective breadboard design parameters are also listed in these tables.

Table 2-1. Electrostatic Analyzer Specifications and Breadboard Design

14881-17R1

CONTRACTUAL SPECS	BREADBOARD DESIGN
ION AND ELECTRON SPECTRA < 100 eV TO 20 KeV	50 eV TO 20 KeV
GEOMETRIC FACTOR $\approx 10^{-5}$ TO 10^{-4} CM ² -SR	6×10^{-4} CM ² -SR
≥ 8 ENERGY CHANNELS	16 CHANNELS
$\leq 2\%$ OVERLAP AT FWHM	$\leq 2\%$ OVERLAP-NO GAPS
SWEEPS OF 1, 5, AND 10s	SWEEPS OF 1, 4, 8, AND 16s
VOLTAGES SETTLED TO 95% BEFORE COUNTING	VOLTAGES SETTLED TO $\geq 95\%$ BEFORE COUNTING
GRID TO REPEL PLASMA SOURCE IONS AND ELECTRONS (< 50 eV)	GRID BIASED AT 50 V
SUN SENSOR TO PROTECT CEM	SUN SENSOR
CMD OVERRIDE OF SUN SENSOR	CMD OVERRIDE
REDUCE UV SCATTERING	SANDBLASTED PLATES
COMMANDABLE CEM BIAS	COMMANDABLE BIAS (8 LEVELS)
THREE-YEAR ON ORBIT LIFE	DESIGNED FOR THREE-YEAR OPERATIONAL LIFE
TELEMETRY	ACCUMULATED COUNTS, ENERGY CHANNEL, STATUS, AND DIAGNOSTICS
< 1.25 W	≤ 1.25 W
< 6 LBS	≤ 6 LBS

Table 2-2. Surface Potential Monitor Specifications
and Breadboard Design

14881-18R1

CONTRACTUAL SPECS	BREADBOARD DESIGN
DIELECTRIC SURFACE POTENTIAL MEASURED WITH ELECTRIC FIELD SENSOR	VIBRATING ELECTRODE ELECTROSTATIC VOLTMETER
POTENTIAL AND POLARITY FROM 100 V TO 20 KV	DUAL RANGE: ± 2 KV ± 20 KV
TWO DIFFERENT DIELECTRICS IN FLIGHT	TWO INSTRUMENTS WITH DIFFERENT DIELECTRICS
CHOICE OF SIX DIFFERENT DIELECTRICS	CHANGE SENSING PLATE TO CHANGE DIELECTRICS
TELEMETRY	SURFACE POTENTIAL, RANGE, DIAGNOSTICS
< 2 W	≤ 1 W
< 3 LBS	≤ 3.5 LBS

Table 2-3. Transient Pulse Monitor Specifications and Breadboard Design

14881-19R1

CONTRACTUAL SPECS	BREADBOARD DESIGN
DIPOLE SENSOR	MONOPOLE (123 CM ² PLATE)
MEASURE RADIATED ELECTROMAGNETIC PULSES	MEASURE ELECTROSTATIC PULSES
MULTIPLE THRESHOLD LEVELS	8-BIT DAC
PARAMETERS MEASURED/1s <ul style="list-style-type: none"> - MAX POSITIVE PEAK AMPLITUDE - MAX NEGATIVE PEAK AMPLITUDE <ul style="list-style-type: none"> - POSITIVE INTEGRAL - NEGATIVE INTEGRAL - PULSE WIDTH - NUMBER OF PULSES 	PARAMETERS MEASURED/1s <ul style="list-style-type: none"> - POSITIVE PEAK AMPLITUDE/PULSE - NEGATIVE PEAK AMPLITUDE/PULSE - INTEGRALS NOT MEASURED - PULSE WIDTH/PULSE - PULSES/SEC
10 V/M TO 10 KV/M FIELD STRENGTH	10 V/M TO 10 KV/M
10 nS TO 10 μ S PULSE WIDTHS	20 nS TO 10 μ S
1 COUNT/mS MAX	1 COUNT/mS
TELEMETRY	PARAMETERS MEASURED AND DIAGNOSTICS
< 3 W	\leq 5 W
< 3 LBS	\leq 3 LBS

Table 2-4. Plasma Source Specifications and Breadboard Design

14881-20R1

CONTRACTUAL SPECS	BREADBOARD DESIGN
< 50 eV NEUTRAL PLASMA	< 40 eV
IONS FROM A NOBLE GAS	XENON
10 μ A, 100 μ A, AND 1 MA ION CURRENT LEVELS (SELECTABLE)	0 TO > 1 MA
≤ 10 s IGNITION	< 1s
1200 HOURS OPERATION	> 1200 HOURS
1000 ON-OFF CYCLES	> 1000 CYCLES
< 25 W	≤ 12 W OPERATING ≤ 20 W CONDITIONING
< 15 LBS	< 15 LBS
BLOW-OFF COVER	MAY NOT BE NECESSARY
TELEMETRY	EMISSION CURRENT AND DIAGNOSTICS

Table 2-5. Controller Specifications and Breadboard Design

14881-21R2

CONTRACT SPECS	BREADBOARD DESIGN
<p>PROVIDE AUTONOMOUS OPERATION OF FMDS</p> <p>DETERMINE IF THRESHOLD LEVELS OF CHARGING HAVE BEEN EXCEEDED</p> <p>TURN-ON PLASMA SOURCE AND OPERATE FOR 5, 10, 30, OR 60 MINUTES</p> <p>DETECT WITH 98% RELIABILITY</p> <ul style="list-style-type: none"> - 95% OF CASES FOR CHARGING ≥ 500 V - 100% OF CASES FOR CHARGING ≥ 1000 V <p>COMMANDABLE THRESHOLD CHARGING LEVELS OF 200, 500, 1000, AND 2000 V</p> <p>SPACECRAFT ARCING TO ACTIVATE PLASMA SOURCE</p> <p>EMI PULSES WITHIN 1s OF SPACECRAFT COMMAND TO BE IGNORED</p> <p>EXTERNAL COMMAND ADJUSTMENT OF TPM ALGORITHM</p> <p>EXTERNAL COMMANDING OF PLASMA SOURCE</p> <p>TELEMETRY</p> <p>DESIGN TO INCLUDE CONSIDERATIONS OF RADIATION HARDENING</p> <p>REDUNDANCY</p> <p>EXCESS CAPACITY</p>	<p>AUTONOMOUS OPERATION</p> <p>CHARGING ABOVE THRESHOLD WILL BE DETECTED</p> <p>TURN-ON AND CONTROL PLASMA SOURCE TURN-OFF BASED ON TIME, EMISSION CURRENT, AND/OR ENVIRONMENTAL CONDITIONS</p> <p>DESIGNED TO MEET BASED ON SC9 DATA</p> <p>SAME</p> <p>ARCING WILL ACTIVATE PLASMA SOURCE</p> <p>ABILITY TO BLANK TPM FOR 1s (REQUIRES SIGNAL FROM SPACECRAFT)</p> <p>ALL ALGORITHMS WILL BE ADJUSTABLE VIA EXTERNAL COMMAND</p> <p>MANUAL OPERATION OF COMPLETE FMDS</p> <p>STATUS AND DIAGNOSTICS</p> <p>HARDENED TO 5×10^5 RADS</p> <p>CRITICAL PARAMETERS STORED IN THREE LOCATIONS (MAJORITY VOTING)</p> <p>EXCESS MEMORY AND I/O</p>

THIS PAGE INTENTIONALLY LEFT BLANK

SECTION 3

PLASMA SOURCE

The FMDS Plasma Source consists of three subsystems: the SPACECLAMP Plasma Generator, the power electronics required to operate and control the Plasma Generator, and the expellant storage and control assembly. The SPACECLAMP Plasma Generator is being developed under a Hughes IR&D project and therefore, specific details of its operation and construction are considered to be proprietary. The expellant storage and control is integral to the rapid-starting capabilities of the Plasma Generator and therefore, specific details on it are also considered proprietary.

3.1 PLASMA GENERATOR

The Plasma Generator is regarded as the major element of the system, since its design and operating characteristics determine the requirements for the other two elements (power supplies and gas supply). The SPACECLAMP Plasma Generator has the general characteristics shown in Table 3-1.

The Plasma Generator consists of a compact arrangement of a hollow-cathode, keeper and anode electrodes, a magnetic field, and a ground shield. Xenon gas flowing through the Plasma Generator is ionized by electron bombardment. The ionized gas flows out of the Plasma Generator, providing a low density ($\approx 10^{10}/\text{cm}^3$), inert-gas plasma which will neutralize differential charge buildup between various surfaces of the spacecraft and will also form an electrically conducting "bridge" between the spacecraft and the natural space plasma. A simple schematic of the Plasma Generator is shown in Figure 3-1.

3.2 EXPELLANT STORAGE AND CONTROL SYSTEM

Xenon is supplied to the Plasma Generator with the arrangement shown in Figure 3-2. The system consists of a Department of Transportation (DoT) approved pressure vessel (rated for transportation on commercial aircraft) which contains 100 standard

Table 3-1. SPACECLAMP Plasma Generator Characteristics

14881-22

PARAMETER	VALUE	UNIT
EXPELLANT FLOW RATE	< 40	mA(EQUIV)
DISCHARGE VOLTAGE	< 40	V
DISCHARGE CURRENT	< 200	mA
KEEPER VOLTAGE	< 25	V
KEEPER CURRENT	< 200	mA
TOTAL POWER (RUN)	< 10	W
TOTAL POWER (ONE-TIME-ONLY CONDITIONING)	20	W
IGNITION TIME	< 1	S
EXPECTED LIFETIME	> 1200	HOURS
EXPECTED RESTART CAPABILITY	> 1000	STARTS
ION-EMISSION CURRENT (MAX)	> 1	mA

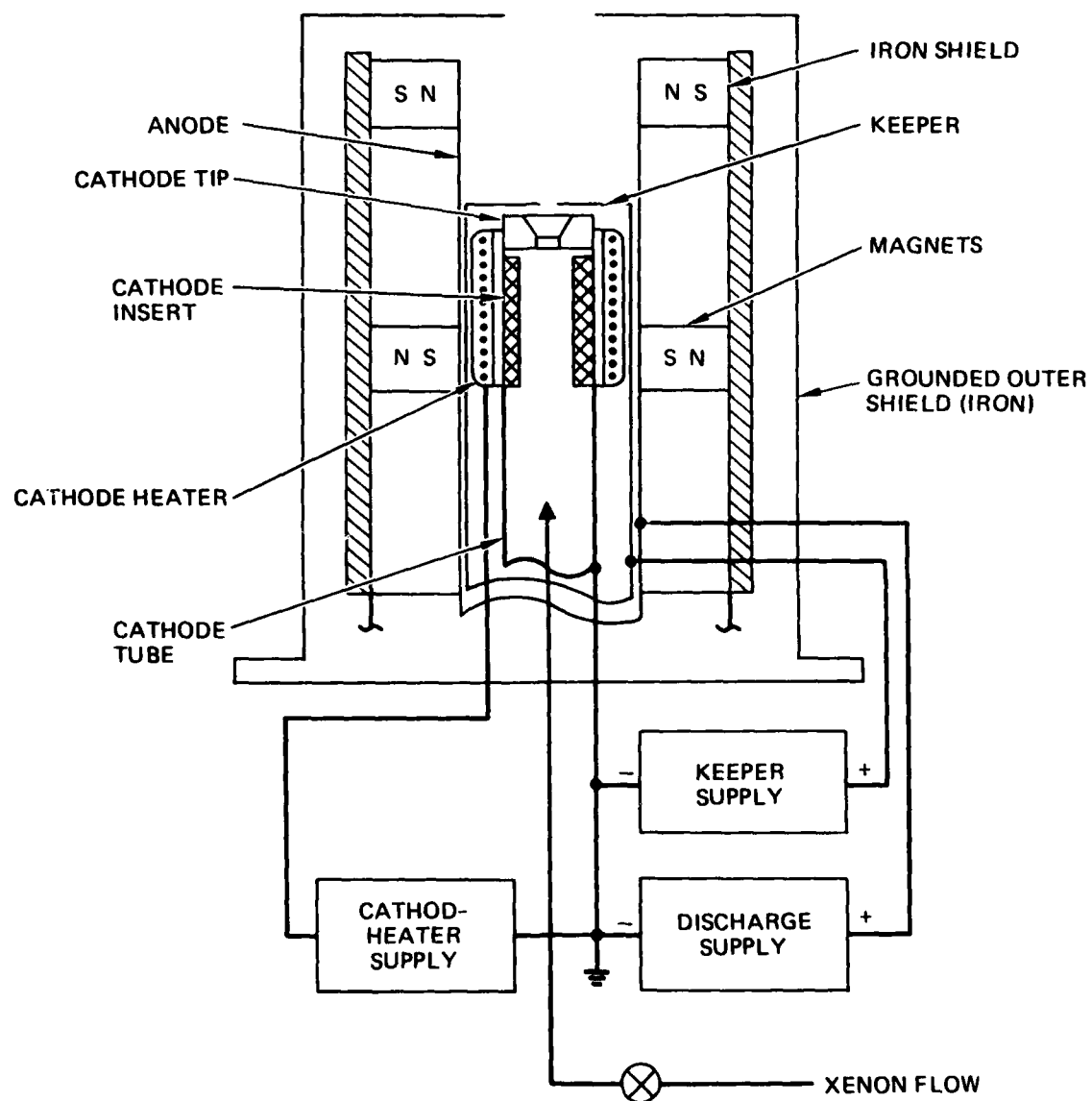


Figure 3-1. Simple schematic of the xenon plasma source.

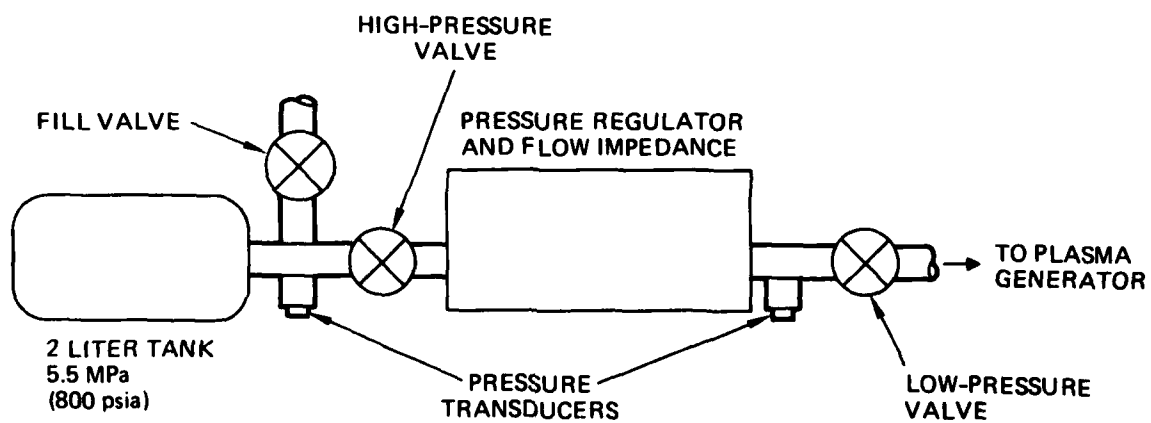


Figure 3-2. Design of the expellant feed system.

liters of xenon at a pressure of 5.5 MPa (800 psia). The tank is fitted with a pressure transducer (to indicate the quantity of remaining expellant) and a manually operated fill valve (per MS28889-2).

Xenon flows from the pressure vessel to the Plasma Generator through a system of valves, a flow impedance, and a pressure regulator. These elements are intended to provide the flow characteristics which are needed by the Plasma Generator.

The Plasma Generator operates at a xenon flowrate of approximately 0.5 SCCM (33.5 mA). To provide this constant flow, we employ a regulator to reduce the pressure to a value of about 70 kPa (10 psia). This constant pressure is maintained on the upstream side of a constant flow impedance to supply the desired flowrate.

In the schematic presented in Figure 3-2, we differentiate between high-pressure and low-pressure valves; these valves are identical latching-solenoid types. Four known sources for latching-solenoid valves were contacted -- manufacturers whose valves have been used in previous flight programs at Hughes Research Laboratories (RL) or other divisions of Hughes. These manufacturers are listed below, along with a brief description of their respective valves.

o Hydraulic Research, Textron Division; Valencia, California

The model TLM-70 valve is used by the Hughes Space and Communications Group and is described as a torquemotor-actuated magnetic latching valve. A torquemotor valve is an actuator in which spring forces and magnetic forces are balanced to yield the desired results. The primary spring in a torquemotor valve is a flexure tube. Like any spring, the flexure tube may be deflected in either direction from a null position, with predictable results. The magnetic circuit is equally predictable, in that an established magnetic circuit will always produce the same force when the air gap is reduced to zero. the magnetic circuit has continuity in both open and closed valve positions, and therefore supplies the same force in both positions.

It has no sliding fits or surfaces except for the self-aligning feature on the poppet. Therefore, it does not generate contamination by surface galling. The manufacturer produces these valves in only one grade (high reliability), with the result that the cost per valve is a major consideration.

- o Futurecraft; City of Industry, California

Futurecraft makes mechanical latching valves only. Under an earlier contract with AFGL (F19628-83-C-0057), RL selected the Futurecraft Model No. 2004B7 for use on the Positive Ion Ejection System (PIES). This valve is large because the latch is actuated at right angles to the valve poppet. We believe that mechanical latching valves are acceptable for several thousand duty cycles, but are more susceptible to galling and contamination than a magnetic latching valve which has half the number of moving parts.

- o Moog-Carlston; East Aurora, New York

Carlston Controls supplied a magnetic latching-solenoid valve and pressure regulators for the Satellite Positive Ion Beam System (SPIBS) which RL developed under contract F19628-76-C-0066 for AFGL. This company is familiar with our requirements for FMDS and would like to supply the entire expellant feed system.

- o Valcor; Springfield, New Jersey

Valcor supplied the magnetic latching-solenoid valves for the feed system used to supply mercury to the ion thrusters on the Ion Auxiliary Propulsion System (IAPS) which was developed at Hughes under contract NAS 3-21055 for NASA's Lewis Research Center. The Model V27200 valves are compact and have been flight-qualified for the Shuttle. Valcor also supplies pressure regulators.

Considering size, weight, cost, and delivery time, the valve and regulator units manufactured by Valcor appear most suitable for this application.

3.3 PLASMA GENERATOR ELECTRONICS DESIGN

The Plasma Generator electronics block diagram is shown in Figure 3-3. It contains a discharge supply, keeper supply, and a heater supply for operation of the plasma source, a bipolar log-

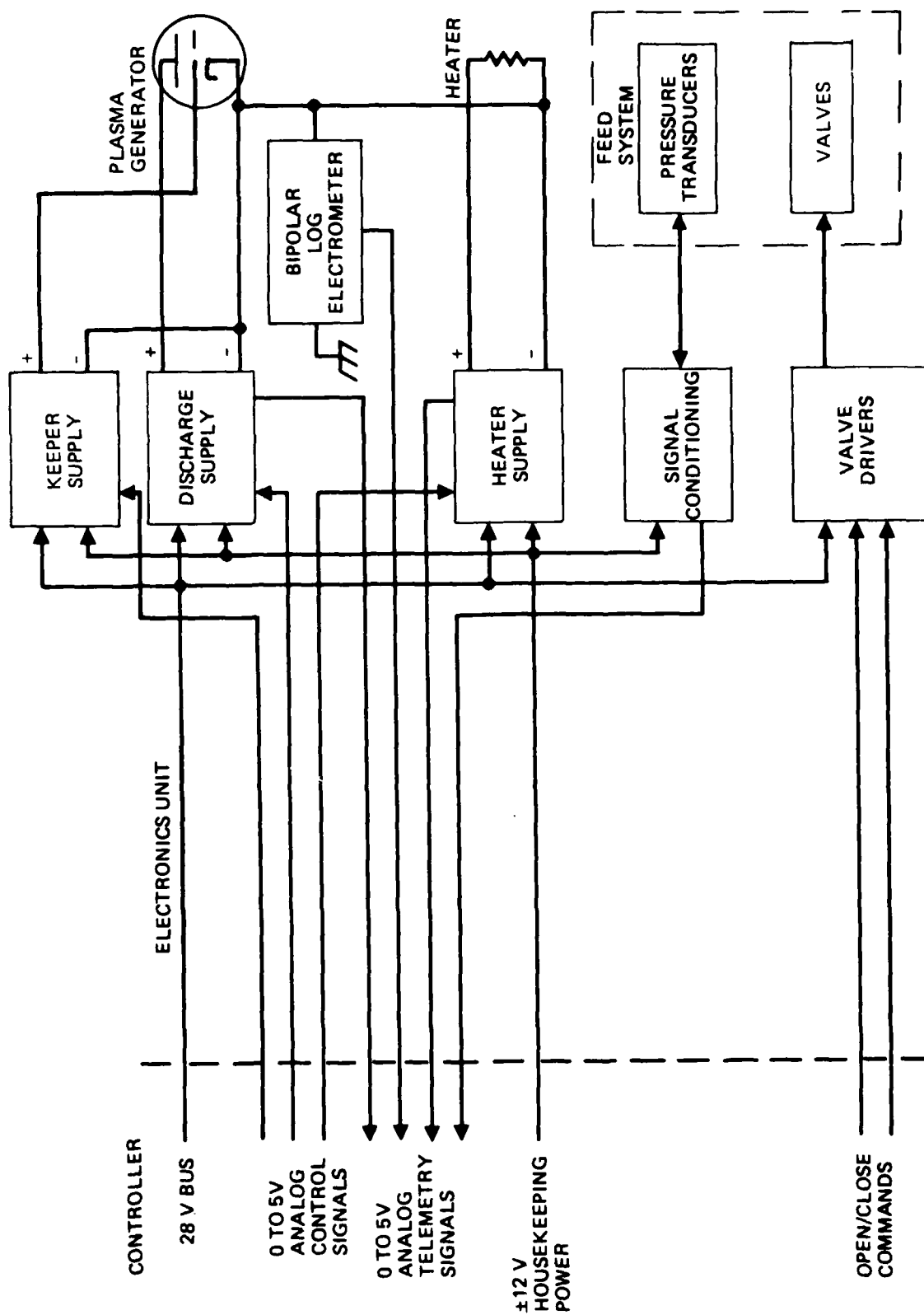


Figure 3-3. Plasma Generator electronics block diagram.

electrometer to measure the emission from the Plasma Generator, valve drivers for the expellent valves, and analog telemetry signal conditioning.

3.3.1 Power Circuitry Options and Tradeoffs

The three Plasma Generator power supplies must provide different dc output voltage and must be electrically isolated from the chassis. Therefore, each supply must include a regulated, isolated, dc-to-dc converter. In our analysis and design of the FMDS, we considered several types of dc-to-dc converters before choosing a specific approach for this application. The various alternative types of dc-to-dc converter configurations available to perform the above conversions are summarized in Table 3-2. Typical performance characteristics of each type are included, with relative values assigned to aid in making an optimum design choice.

The Plasma Generator power requirements are relatively low (<20 W max), which rules out the need for a complex, multi-stage converter. Therefore, we chose the simplest converter, the Half-Wave Flyback design (Figure 3-4) for all three supplies. It offers many significant advantages over the other available power supply designs. It is the simplest type which provides isolation and high reliability while requiring a minimum number of components. Since it operates in a current-source mode rather than a voltage-source mode it exhibits inherent output short-circuit protection. Only four power-handing components are required:

- o One transformer (T1)
- o One transistor switch (Q1)
- o One blocking diode (CR1)
- o One filter capacitor (C1).

The flyback inverter functions by cyclically storing energy in the magnetic field of transformer T1 while Q1 is turned ON and

Table 3-2. Dc-to-dc Converter Characteristic Comparison

14881 23

CONVERTER TYPE	TRANSISTORS	COMPLEXITY/RELIABILITY	APPROXIMATE POWER LIMIT	REGULATION	OVERLOAD-SHORT CIRCUIT PROTECTION	EFFICIENCY
FLYBACK-HALF WAVE	ONE	1	100 W	1	1	2
FEED-FORWARD	ONE	2	200 W	1	3	2
BLOCKING OSCILLATOR	ONE	1	100 W	2	3	2
C'UK (WITH TRANSFORMER)	ONE	2	100 W	1	2	1
FULL WAVE FLYBACK	TWO	2	200 W	1	1	2
PUSH-PULL, SQUARE WAVE	TWO	2	200 W	1	3	2
CURRENT FED PUSH-PULL, SQUARE WAVE	TWO	2	500 W	1	3	2
		1 - SIMPLE, HIGH RELIABILITY		1 EXCELLENT	1 INHERENT/CURRENT SOURCE	1 EXCELLENT
		2 - MEDIUM, MEDIUM RELIABILITY		2 FAIR	2 - IMPEDANCE LIMITED	2 - FAIR
		3 COMPLEX, LOW RELIABILITY		3 POOR	3 REQUIRES EXTERNAL ACTIVE SENSING & CONTROL	3 - POOR

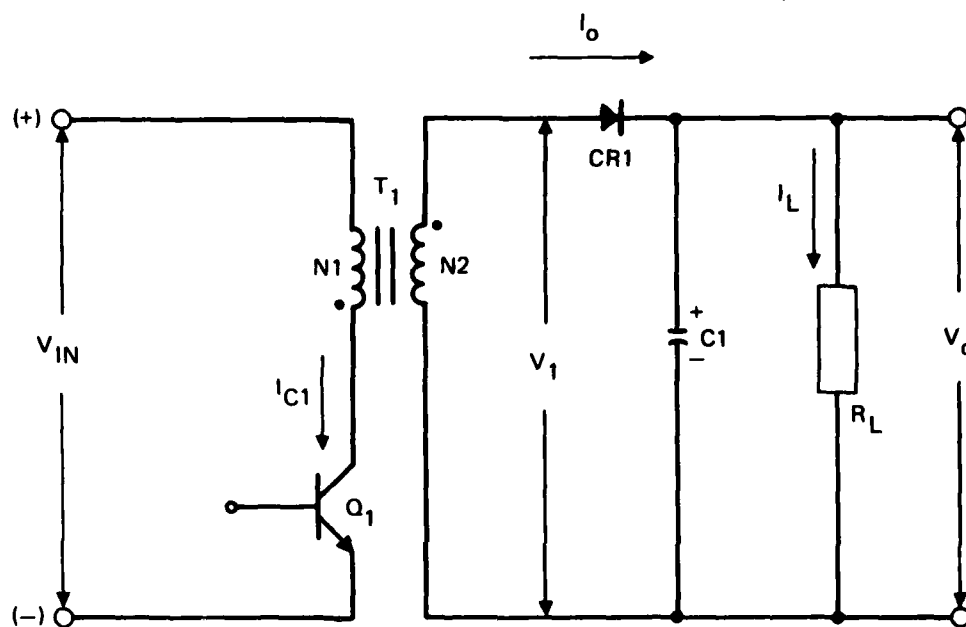


Figure 3-4. Simplified schematic of a half-wave flyback inverter.

then transfers this stored energy to T1's secondary through diode CR1 to the output filter (C1) and the load when Q1 is OFF. By varying the Q1 ON time, the amount of energy stored and transferred to the load in each cycle can be controlled or regulated in proportion to changes in input voltage, output load, or commanded setpoint.

The operation of a flyback inverter is basically single ended. Voltage is applied to transformer T1 in only one polarity and then returned to zero. The resultant magnetic flux in T1 also operates in only one polarity and resets back to zero. Only one-half of the available core flux is utilized in each cycle, which dictates the use of a core with at least twice the cross-sectional area as compared with a double-ended-transformer design.

Flyback inverters impose constraints on the switching element (Q1) due to the highly inductive load that transformer T1 represents. The transistor must turn OFF while the transformer current is at its maximum, causing a rapidly increasing inductive voltage to be imposed across the transistor which is limited only by the external circuitry. The simultaneous high-voltage and high-current transient imposed on the transistor can cause a potentially dangerous hot spot in bipolar transistors known as second breakdown. The voltage and power rating of bipolar transistors used in flyback inverters must, therefore, normally be considerably overrated for reliable operation. However, recently developed MOSFET power transistors do not exhibit this thermally-induced secondary-breakdown phenomena and are much more suitable for flyback inverter applications. The MOSFET switch can be utilized at its full-rated drain-source voltage (BV_{DS}), while the bipolar transistor is limited to operation at less than one-half of its full-rated collector-emitter voltage (BV_{CES}). Additional desirable features of the MOSFET are: faster switching speeds allowing higher inverter operating frequencies, smaller magnetic and capacitive filter components, and simpler gate-drive circuitry due to the very high gate impedance ($>10^8 \Omega$).

3.3.2 Bipolar Log Electrometer

The bipolar log electrometer schematic is shown in Figure 3-5. It measures currents in the range of $-1\ \mu\text{A}$ to $-10\ \text{mA}$ and $1\ \mu\text{A}$ to $10\ \text{mA}$. It has a 0 to 5-V analog telemetry output with zero out corresponding to $-10\ \text{mA}$, 2.5-V out corresponding to $-1\ \mu\text{A}$ to $1\ \mu\text{A}$, and 5-V out corresponding to $10\ \text{mA}$.

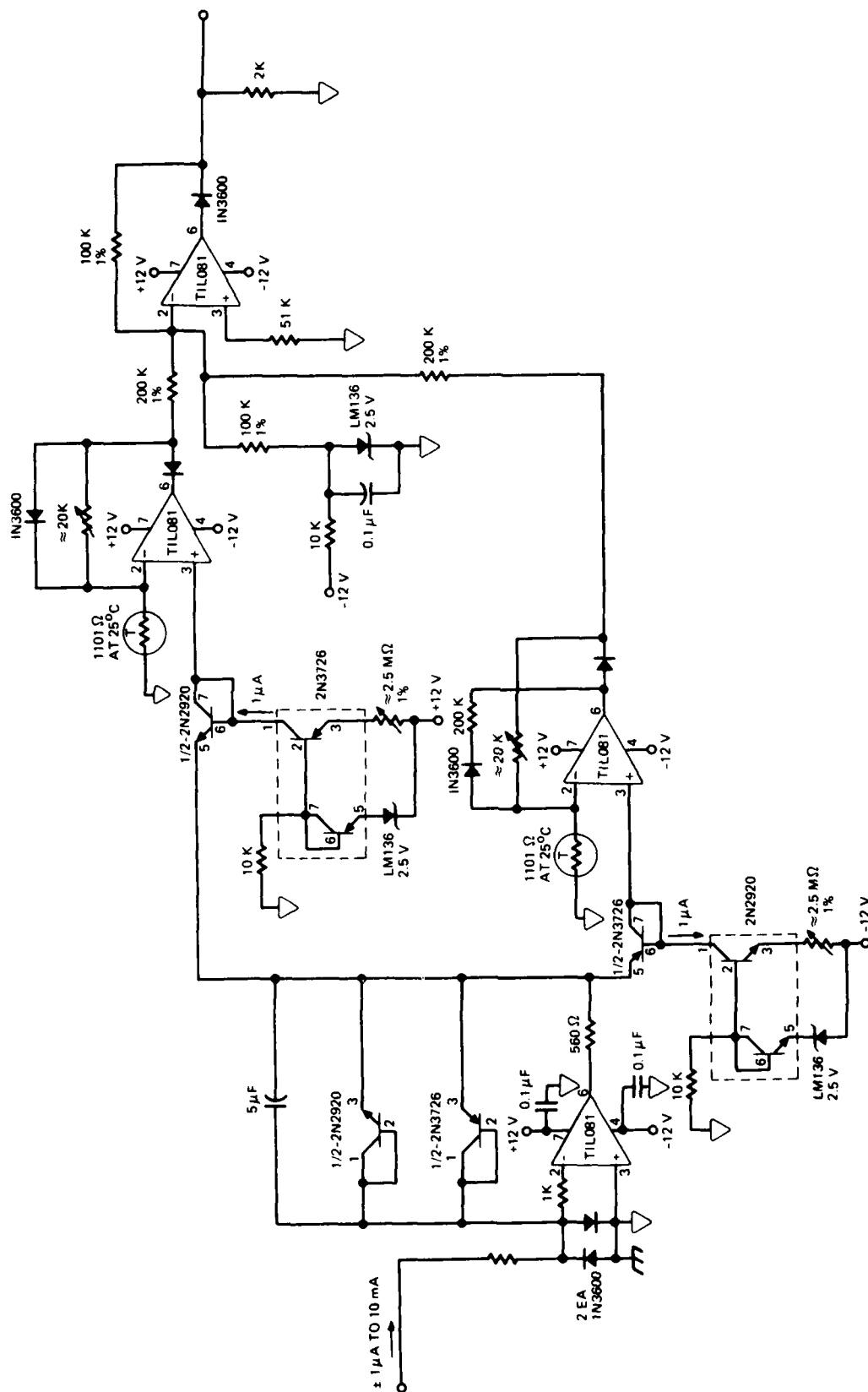


Figure 3-5. Bipolar log electrometer schematic.

THIS PAGE INTENTIONALLY LEFT BLANK

SECTION 4

ELECTROSTATIC ANALYZERS

The FMDS incorporates ESAs to measure the distribution of ion and electron energies which are incident on the spacecraft. This instrument is of pivotal importance to the FMDS charging-detection function because it is the only instrument of those specified for FMDS which can detect the onset of eclipse charging (the SPMs respond too slowly when the spacecraft is in darkness). In addition to these important charging-detection attributes, the ESAs provide valuable scientific information: its data can be analyzed to determine the actual vehicle potential (i.e., frame potential relative to space potential) rather than the dielectric-surface potentials monitored by the SPMs.

The ESAs that are employed on the FMDS are configured with short-cylindrical-section sensors. Instruments of this type have been used in physics experiments since the turn of the century, and similar devices have been flown on many spacecraft. The FMDS instrument incorporates 16 channels and fast sweep times in order to provide the rapid reaction time that is required in the FMDS mission.

The electrostatic analyzers for the FMDS have been provided by Panametrics Inc. of Waltham, MA under subcontract.

4.1 CYLINDRICAL-ESA OPERATING PRINCIPLES

Figure 4-1 shows a schematic diagram of a typical ESA. Protons of energy $W = mv^2/2$ enter a collimating structure (which defines the cone of angles that is accepted into the analyzer) and then pass into the space between two metal plates which are curved with a common center of curvature, a separation, S , and a mean radius of curvature, R . An electric field, $E = V/S$ (where V is the potential difference between the plates), is maintained between the plates so that incident protons experience a radially inward force, $F_{in} = qE$, where q is the proton charge. Since the ions are moving in a curved path, they also experience a radially outward centrifugal force, $F_{out} = mv^2 \hat{R}/R$, where \hat{R} is the unit vector in the radial direction. In general, particles

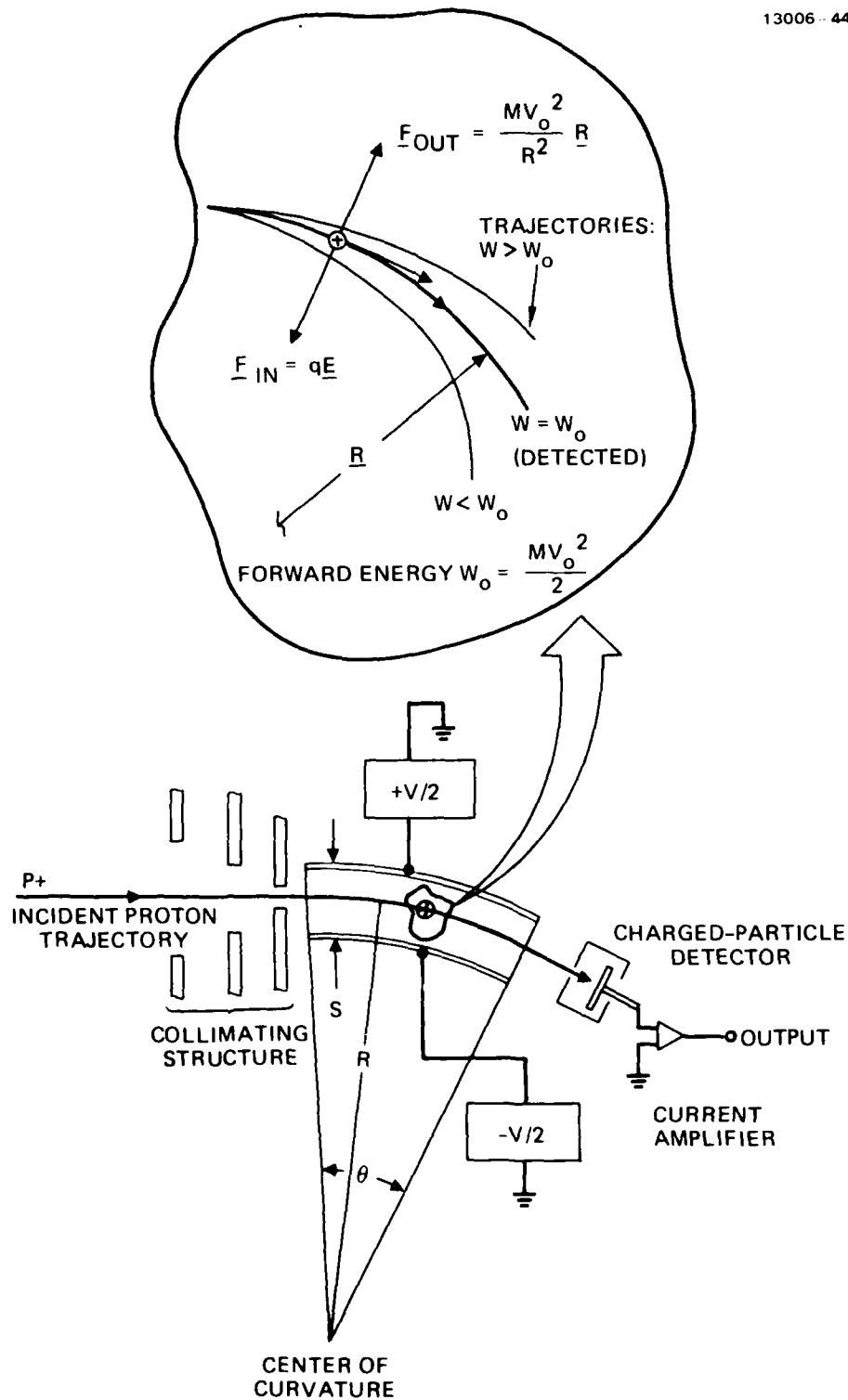


Figure 4-1. ESA operating principles.

traversing the analyzer will experience an imbalance between the two radial forces just identified; these particles will follow trajectories with radii of curvature different from R . These trajectories impact the analyzer plates, as shown in Figure 4-1. For the small class of particles for which $\underline{F}_{in} = \underline{F}_{out}$, however, the trajectories follow the center of the analyzer exactly, reaching the particle detector at the end of the analyzer. This class of particles is characterized by an energy, $W_0 = mV_0^2/2$, and they are detected when $V = 2W_0 S/qR$. Physically, this can be thought of as meaning that the particles have received a sideways energy gain, qV , which is just $2S/R$ of their forward-directed energy, W_0 . This fractional sideways energy is precisely the amount required to generate a trajectory that reaches the particle detector.

Notice that if $S \ll R$, then the voltage on the plates, V , can be very much less than W/q . This is an important advantage of the electrostatic analyzer because reasonable plate voltages, V , can be used to detect very energetic particles.

Also notice that the condition given above for particle detection is independent of the angular extent, θ , of the analyzer. Analyzers of larger angular extent detect the same-energy particles, but with increased dispersion; that is, particles with an energy W that differs slightly from the resonant energy, W_0 , will accumulate larger radial displacements from the resonant trajectory. For a given particle-detector aperture size, smaller and smaller deviations from the resonant energy, W_0 , will lead to particles missing the detector entrance aperture as the analyzer angular extent, θ , is increased.

Increased ESA dispersion provides superior energy resolution, but this gain is at the expense of the particle counting rate. Low particle counting rates require longer integration times per channel to obtain a given statistical validity.

4.2 ESA DESIGN

The ESA design is for 15 energy channels plus a background channel, making a total of 16. The background channel is important because it allows direct subtraction of the scattered electron background in the lower energy channels for more reliable spacecraft charging measurements. Table 4-1 lists the basic specifications for the ESA design, and Table 4-2 lists the energy detection characteristics of the ESA. The following Sections describe the design in more detail.

4.2.1 Detection Assembly Design

The basic design of the ESA detection assembly is shown in Figure 4-2. The assembly is similar to several that have been constructed by Panametrics, so it is a proven design with well-known detection characteristics. The unit has been designed for satellite use, and so can withstand the shock, vibration, and other environmental aspects of launch and orbital operations. The major characteristics of the detection assembly are described below.

- o The analyzer plates have a narrow separation, and the surfaces are treated to reduce particle and light scattering. This is important to reduce electron background from the scattering of the intense high energy (tens of keV) electron fluxes present during spacecraft charging events. This unit should readily detect the proton charging peak in the presence of intense electron fluxes. The plate design also strongly reduces the intensity of scattered solar UV reaching the CEM detector.
- o The CEM and associated electronics are mounted on a ceramic circuit board. This reduces the level of organic vapors near the CEM, and so helps prolong its life. Since the CEM is the component most likely to degrade, considerable care must be used to minimize organic contamination, which tends to hasten CEM gain degradation.

Table 4-1. Basic Specification for the ESA Design

14881-24

PARAMETER	SPECIFICATION
PARTICLES DETECTED	IONS AND ELECTRONS
GEOMETRIC FACTOR	BETWEEN 10^{-5} AND 10^{-4} CM ² -SR
NUMBER OF ENERGY CHANNELS	MINIMUM OF 8
NOMINAL UPPER EDGES AT FWHM	100 eV, 200 eV, 500 eV, 1 KeV, 2 KeV, 5 KeV, 10 KeV, AND 20 KeV
ADJACENT CHANNEL OVERLAP	0 TO 2% AT FWHM
TIME PERIOD FOR FULL ENERGY SWEEP	MINIMUM OF 1 SEC, 5 SEC, AND 10 SEC. CHANGE OF SWEEP PERIOD RESULTS IN RE-START IN FIRST CHANNEL
SETTLING TIME BETWEEN CHANNELS	VOLTAGES TO AT LEAST 95% OF OPERATING VALUE
LOW ENERGY ION CUT-OFF	50 eV TO AVOID COUNTING PLASMA SOURCE IONS
SUN SENSOR	REDUCES ELECTRON MULTIPLIER GAIN WHEN VIEWING THE SUN. CAN BE OVERRIDDEN BY COMMAND
ELECTRON MULTIPLIER GAIN CONTROL	BIAS VOLTAGE CAN BE CHANGED BY COMMAND TO OFFSET EFFECTS OF DEGRADATION
DESIGN LIFETIME	MINIMUM OF THREE YEARS IN FMDS APPLICATION
DIGITAL (BILEVEL) OUTPUTS TO CONTROLLER	ACCUMULATED COUNTS; ENERGY CHANNEL
DIGITAL (BILEVEL) OUTPUTS TO TELEMETRY	ACCUMULATED COUNTS; ENERGY CHANNEL; SWEEP PERIOD; SUN SENSOR; DETECTOR VOLTAGE LEVEL
ANALOG OUTPUTS TO TELEMETRY	APPROPRIATE DIAGNOSTICS
POWER CONSUMPTION	1.25 WATTS
WEIGHT	6 LBS

Table 4-2. Energy Detection Characteristics of ESA

14881-25R1

CHANNEL NUMBER	ENERGIES IN eV		
	E (LOW)	E (HIGH)	E (AVERAGE)
1	BACKGROUND CHANNEL		
2	50	75	62
3	75	111	93
4	111	166	138
5	166	247	206
6	247	368	308
7	368	549	459
8	549	819	684
9	819	1221	1020
10	1221	1821	1521
11	1821	2714	2267
12	2714	4047	3381
13	4047	6034	5041
14	6034	8997	7516
15	8997	13414	11205
16	13414	20000	16707
GEOMETRIC FACTOR $6 \times 10^{-4} \text{ cm}^2 - \text{sr}$ (CAN BE MADE SMALLER)			
INTRINSIC ENERGY RESOLUTION $\Delta E (\text{FWHM})/E (\text{AVERAGE}) = 39\%$			

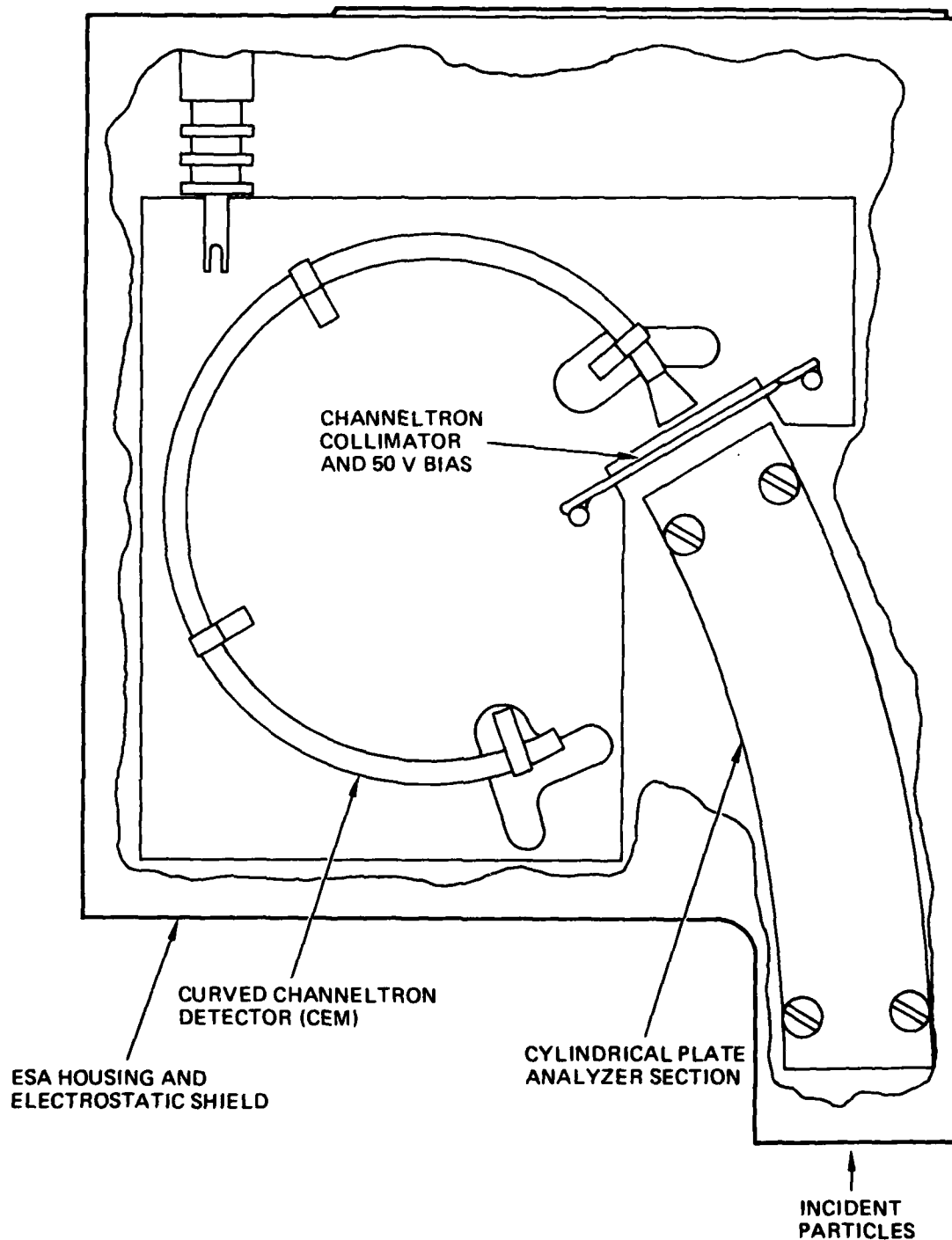


Figure 4-2. Basic design of the electrostatic analyzer detection assembly.

- o The CEM ceramic board is easily replaced so that routine refurbishing of the FMDS could easily include replacement of a partially degraded CEM. Since CEM exposure to organic vapor occurs primarily during exposure to the atmosphere in the pre-launch and post-return environments, a CEM in an FMDS which has experienced several launch/recovery cycles will degrade faster than one which remains in orbit.
- o The ESA has a geometric factor of about $6 \times 10^{-4} \text{ cm}^2\text{-sr}$, which can be readily reduced if desired for low earth orbit applications.

The physical design of the complete ESA unit is shown in Figure 4-3. The ESA, photodiode, and electronics are all contained in a 4.5 x 6 x 5.5-in. housing. The ESA and photodiode apertures must have a clear view of the external particle fluxes. The housing contains connectors for power and information flow to/from the controller.

4.2.2 Electronics Design

The basic electronics design for the ESA is shown in Figure 4-4. The design shows how the basic required operational characteristics are met. Significant features of the design for protons (electrons) include:

- o A +50 V (-50 V) grid in front of the CEM to eliminate protons (electrons) below 50 eV, thus protecting the CEM from the plasma source ions (electrons).
- o A CEM aperture biasing of -500 V (+500 V) to increase the detection efficiency for low energy protons (electrons). This voltage is held fixed to avoid efficiency changes with CEM gain-voltage changes.
- o Adjustable CEM gain by command using a controlled high voltage power supply (HVPS).
- o Reducible CEM gain when the unit looks toward the sun, by means of the photodiode. This operation can be enabled or disabled by command.
- o CEM counts which are accumulated in a 16-bit counter. This allows the CEM to operate at 1 MHz for the 1-s accumulation time, and at 60 kHz for the 16-s accumulation time, based on 16 channels.

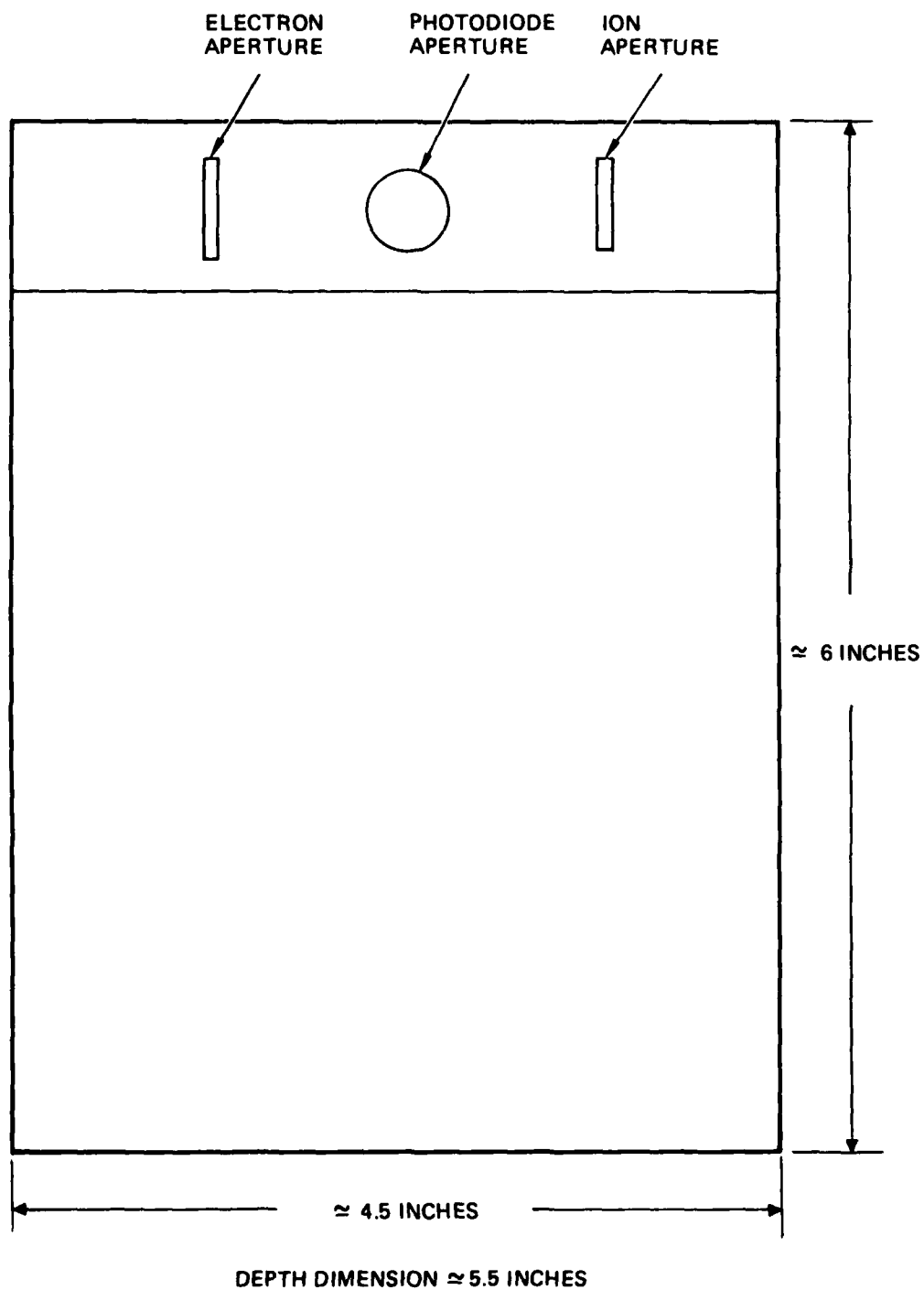


Figure 4-3. General physical design of the entire ESA package.

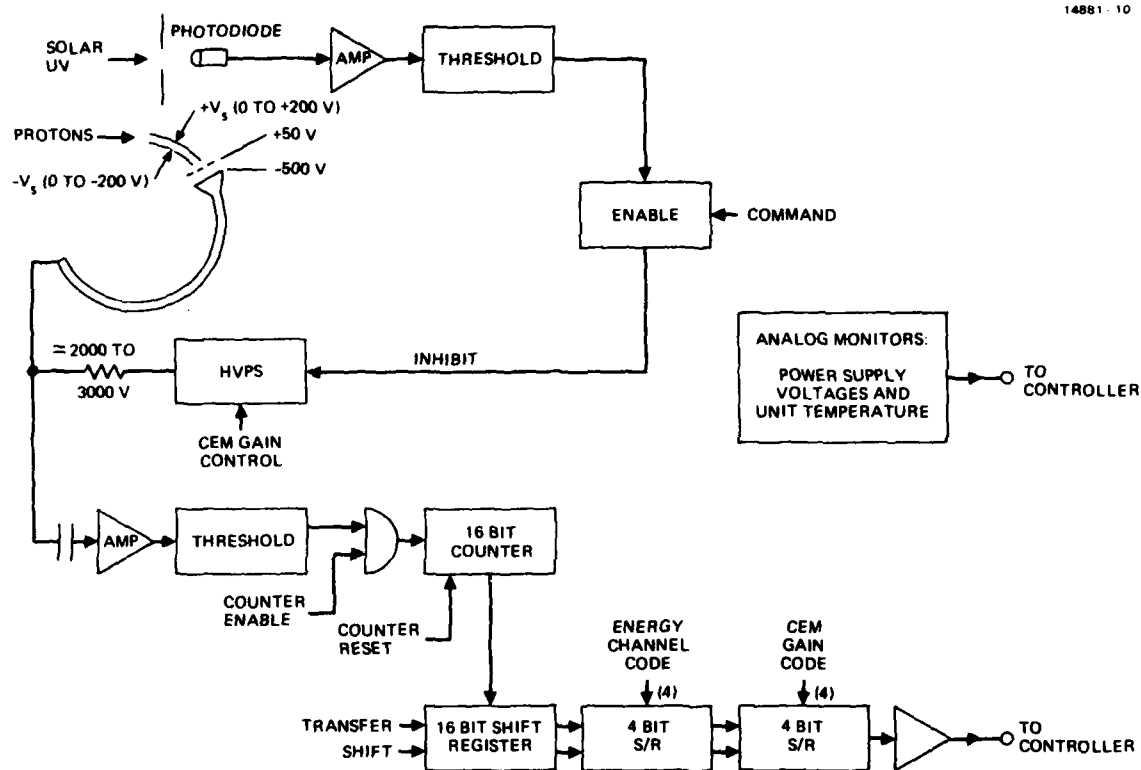


Figure 4-4. Basic design of the ESA electronics for the ion detection head (electron detection electronics are similar except for the polarity of some voltages).

The details of the ESA-plate voltage-sweep control are shown in Figure 4-5. The control voltage drives a bipolar supply to provide $+V_s$ and $-V_s$ in Figure 4-4. The ESA design is such that for 20-keV ions, $\pm V_s = \pm 200$ V. The sequencing in Figure 4-5 is such that R_1 through R_{16} set up the central energy of each energy channel. The value of R_1 is set so that Channel 1 measures background, with no direct ion (electron) response. The circuitry can be readily set to give the energy channels of Table 4-2.

The remainder of the electronics design is straightforward digital control circuitry, timing circuitry, power supplies and interface buffers. The ESA digital commands and telemetry data are given in Tables 4-3 and 4-4, respectively. Analog telemetry data for housekeeping voltages and temperature are also available.

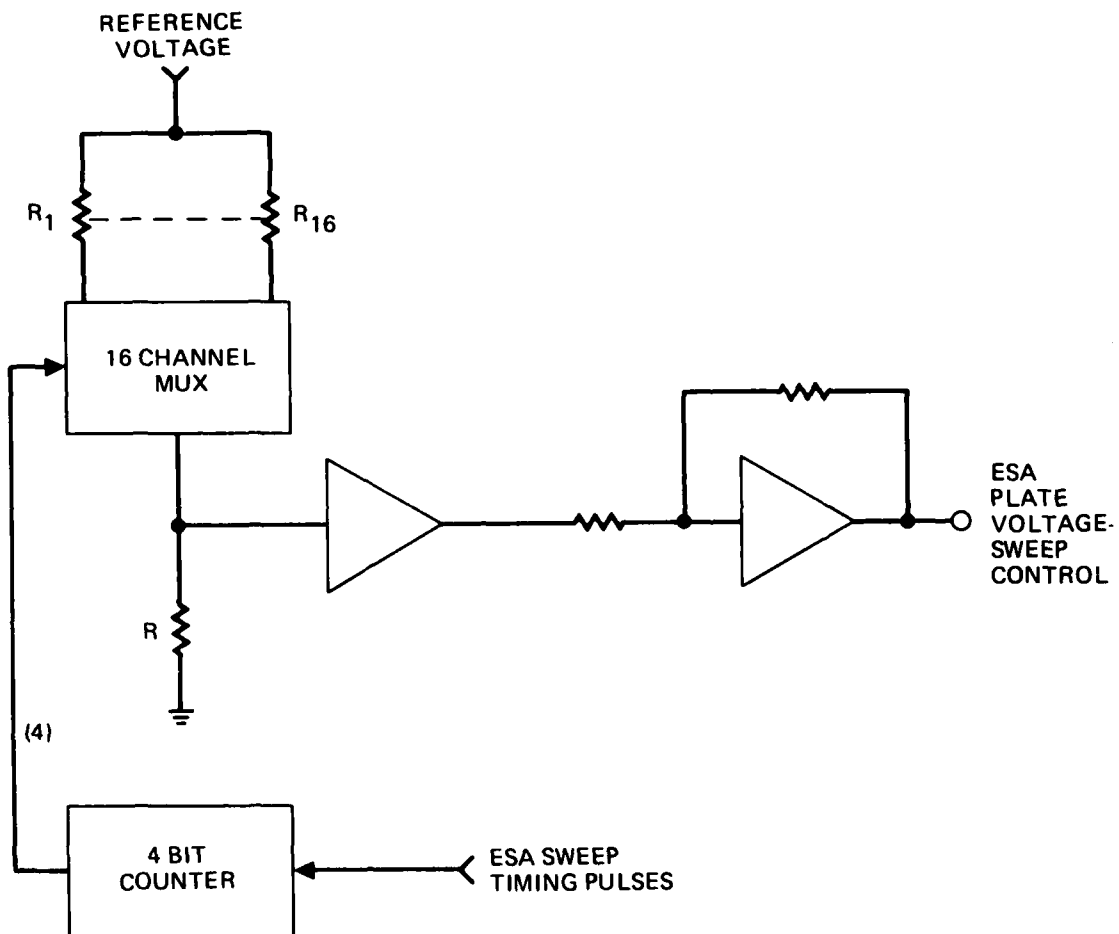


Figure 4-5. Electronic design of the ESA-plate voltage-sweep control.

Table 4-3. ESA Commands Format

14881-26

ESA COMMANDS

9/24/84

ION OR ELECTRON CEM BIAS	MSB BIT 2	BIT 1	LSB BIT 0
LOWEST BIAS	0	0	0
	0	0	1
	0	1	0
MONOTONICALLY INCREASING	0	1	1
	1	0	0
	1	0	1
	1	1	0
HIGHEST BIAS	1	1	1

SWEEP TIME	MSB BIT 1	LSB BIT 0
1 s.	0	0
4 s.	0	1
8 s.	1	0
16 s.	1	1

PHOTO DIODE	1 BIT
ENABLED	0
DISABLED	1

NOTE: ALL SIGNALS ARE POSITIVE TRUE ("1").

Table 4-4. ESA Data Format

ESA DATA

14881-27

9/24/84

ENERGY CHANNEL	MSB BIT 3	BIT 2	BIT 1	LSB BIT 0
0 - LOWEST ENERGY	0	0	0	0
1	0	0	0	1
2	0	0	1	0
3	0	0	1	1
4	0	1	0	0
5	0	1	0	1
6	0	1	1	0
7	0	1	1	1
8	1	0	0	0
9	1	0	0	1
10	1	0	1	0
11	1	0	1	1
12	1	1	0	0
13	1	1	0	1
14	1	1	1	0
15 - HIGHEST ENERGY	1	1	1	1

SWEEP TIME	MSB BIT 1	LSB BIT 0
1 s.	0	0
4 s.	0	1
8 s.	1	0
16 s.	1	1

Table 4-4. Continued

14881-28

ESA DATA - CONTINUED

9/24/84


ION OR ELECTRON CEM BIAS	MSB BIT 2	BIT 1	LSB BIT 0
LOWEST BIAS  MONOTONICALLY INCREASING HIGHEST BIAS	0	0	0
	0	0	1
	0	1	0
	0	1	1
	1	0	0
	1	0	1
	1	1	0
	1	1	1

PHOTO DIODE STATUS	1 BIT
ENABLED	0
DISABLED	1

SWEEP TIME RESET FLAG	1 BIT
NORMAL	0
RESET OCCURRED	1

PHOTO DIODE INHIBIT FLAG	1 BIT
NORMAL	0
INHIBIT OCCURRED	1

Table 4-4. Concluded

14881-29

DATA OVERRUN FLAG	1 BIT
NORMAL	0
OVERRUN OCCURRED	1

ION OR ELECTRON COUNT HIGH BYTE	
BIT WEIGHT	BIT
256	0 - LSB
512	1
1,024	2
2,048	3
4,096	4
8,192	5
16,384	6
32,768	7 - MSB

ION OR ELECTRON COUNT LOW BYTE	
BIT WEIGHT	BIT
1	0 - LSB
2	1
4	2
8	3
16	4
32	5
64	6
128	7 - MSB

NOTE: ALL SIGNALS ARE POSITIVE TRUE ("1").

SECTION 5

SURFACE POTENTIAL MONITORS (SPMs)

Two Surface Potential Monitors (SPMs) are included as part of the FMDS to detect the charging of dielectric surfaces on the satellite. Since two different dielectric materials are to be used in flight, and since it is desirable to have them physically separated (to minimize their effect on each other), the best approach was to use two instruments, with the dielectric material being the only difference (see Figure 2-2).

One of the main factors in the design of the SPMs is the requirement of not altering the charge buildup of ions or electrons on the dielectric material due to the measurement. This dictates that some type of electric-field-sensing device be used.

Most electrostatic voltmeters that have sufficient accuracy and resolution use a field-sensing probe that is closed-loop controlled to the same potential as the surface being measured. In this way the field sensor need only detect a null. To use this approach in this application a "servo-amplifier" with an output of ± 20 kV would be required which is not practical within the weight and power limitations for this instrument. We have chosen, therefore, to use the approach that was adopted by NASA's Lewis Research Center for their surface-voltage sensor (SVS).¹ NASA's approach retains most of the advantages of a feedback sensing system, yet does not require high voltage. This system uses a combination of electrodes that attenuate the field produced by the sensing surface and allow it to be nulled with a low-voltage feedback signal.

We have slightly modified the specifications for the SPMs that were called out in the original RFQ issued by AFGL. The RFQ called for measurement over a range of 100 V to 20 kV and determination of polarity. If 8 bit digital data were used, then the resolution for a 20-kV full scale range would be 78 V, which is rather coarse when looking for surface potentials of 200 V. Therefore, we are using a dual range instrument with nominal ranges of 0 to ± 2 kV and 0 to ± 20 kV. These ranges provide a resolution of 8 V and measure potentials to ± 20 kV.

5.1 DESIGN PHILOSOPHY FOR THE SPM SENSOR HEAD

Since the SPMs will be required to survive vibration and shock experienced during launch, an ideal design would be all solid state; i.e., no moving parts such as a tuning fork. Therefore, several potentially feasible design principles were investigated, as part of Hughes' design study, such as modulation of a light beam within a fiber optic bundle by the E-field and semiconductor-conductivity modulation by the E-field similar to the operation of Field Effect Transistors. However, these ideas would have required considerable development and testing to achieve the level of flight readiness required by the FMDS program. We therefore decided to utilize the most mature technology available at this time: the NASA LeRC vibrating electrode approach.

The availability of the NASA design (Ref. 1) put us in the fortunate position that we not only could adopt this design with only minor modifications, but we could also take a critical look at the important features of this design and propose modifications where we saw an opportunity for worthwhile improvements.

A schematic cross section of the NASA design is shown in Figure 5-1. Inspection of this figure, as well as of the sample SPM sensor head received from NASA, shows that the tuning fork is split into two halves that are then welded to a mounting plate which also serves as a shield between sensing and driving elements. Interspersing two welds into the vibrating element is a less-than-optimum feature of this design - a fact that was also confirmed by the reported failure of some devices to perform properly. This weakness was remedied by welding a one-piece tuning fork to the end of the mounting plate.

We also installed an additional grounded-shield electrode between the compensating electrode ("aperture plate") and the sensing electrode. This prevents any spurious coupling into the

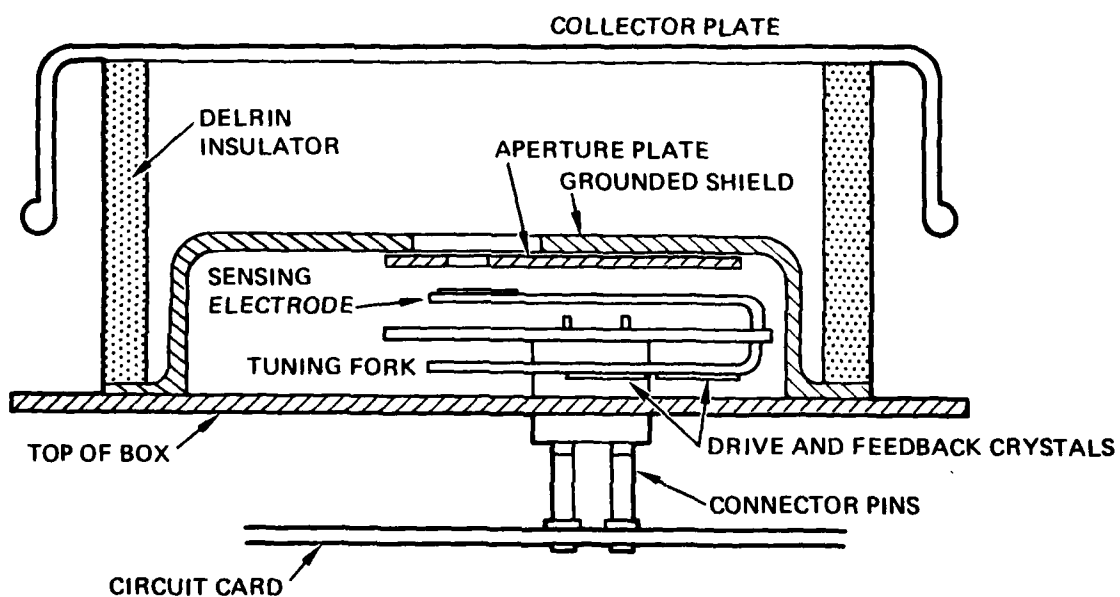


Figure 5-1. NASA surface voltage sensor head detail.

sensing-electrode leads of the electric field emerging from the compensating electrode. This additional electrode also renders less critical the centering of the sensing electrode (bonded to and electrically isolated from the tuning fork) relative to the apertures in the compensating electrodes. Without the additional shield, the instrument's calibration depends not only on geometric parameters that are easily fixed by spacers and jig-enforced concentricity, but also on the exact placement of the bonded components, the location of which is defined with much less precision.

In the NASA design, range switching requires switching between two different sensing electrodes that view the input electrode ("collector plate") through two apertures of different diameter. Thus, switching occurs at the most perturbation-prone point of the amplifier chain (i.e., the high-impedance input). We have alleviated this potential problem, as well as the ones described above, by modifying the SPM sensor-head design to have the following features:

- o A single, circular sensing electrode is employed that utilizes the full width of the tuning fork.
- o Range switching is accomplished by using two compensating electrodes with concentric apertures of different size. Both of these electrodes are connected to the compensating voltage to obtain the high range, while one of them is grounded to obtain the low range. Switching thus occurs only at the output of the circuit that supplies the compensating voltage.
- o Four plates with circular, concentric apertures are located between the input electrode and the sensing electrode, as illustrated by Figure 5-2. The two compensating electrodes are sandwiched between grounded shields.

To provide compensating-voltage multiplication factors of 200 in the low range and 2000 in the high range, typical values of the crucial parameters (diameters d and separation s) in this proposed SPM sensor head design are as follows (see Figure 5-2 for notation): $d(c) = 8.4$ mm, $d(d) = 8.7$ mm, $d(e) = 11.9$ mm, $d(f) = 20$ mm, $d(g) = 22$ mm, $s(b-d) = 27.6$ mm.

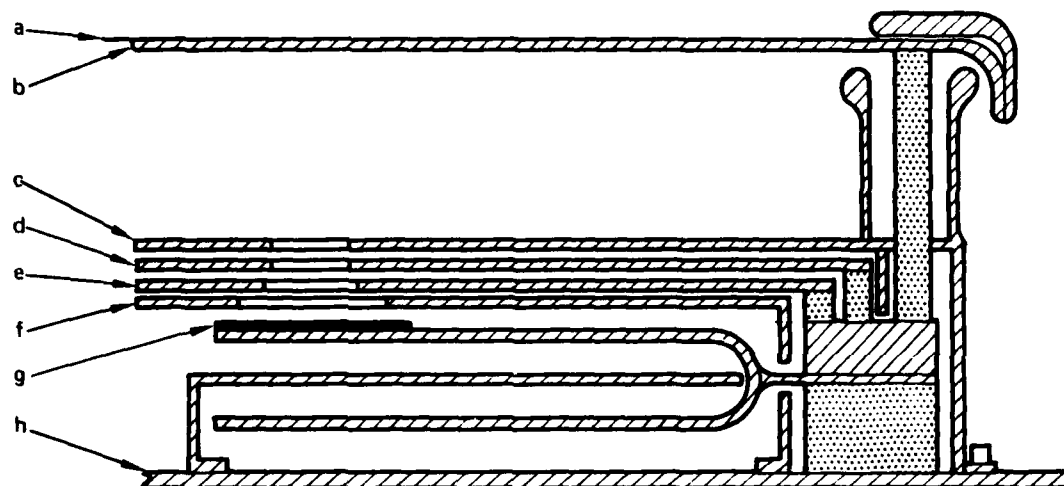


Figure 5-2. Schematic cross section of Hughes SPM sensor head redesign (not to scale).

a = dielectric sample, b = input electrode, c = grounded shield, d = 1st compensating electrode, e = 2nd compensating electrode (ground for low range), f = grounded shield, g = sensing electrode (bonded to tuning fork), h = grounded mounting plate.

The scaling for this design has been derived by adapting the theory of control-grid amplification factors for electron tubes (Ref. 2) to the present geometrical situation. That theory, in turn, represents a highly complex application of the theory of electrostatic potentials. The equation used is

$$\mu = \frac{2\pi sL - \ln \cosh \pi F}{\ln \coth \pi F} ,$$

where

μ = voltage multiplication factor,

s = $s(b-d)$ in Figure 5-2,

L = (circumference of compensating electrode aperture)/(total area of compensating electrode, including aperture, exposed to sensing electrode),

F = screening fraction (exposed area of compensating electrode without aperture)/(total exposed area of compensating electrode, including aperture).

This equation can only be expected to yield approximate dimensions because it is being applied beyond the validity limits of several underlying simplifying assumptions. More accurate equations would fill half a page and still be only approximations. Thus, some experimentation with dimensions is inevitable.

However, one implication of the above equation, i.e., the non-dependence of μ on the spacing between sensing and compensating electrodes, is believed to be fairly valid for the given application where the sensing electrode performs an averaging function for all charges induced on its surface. (This is not the case with electron tubes, where electron emission can vary locally across the cathode surface.)

To the degree that a residual dependence of μ on the spacing between sensing and compensating electrodes does exist, a certain amount of inherent temperature compensation for the instrument's calibration can be provided by mounting the input electrode and

the two compensating electrodes off a reference plane that coincides with the rest position of the sensing electrode, using standoff insulators made of the same material for all three electrodes (see Figure 5-2).

The validity of the above equation for μ was checked by applying it to the existing NASA design. Here, because of the lack of a limiting aperture between sensing and control electrodes, a correction factor for the field spreading between these electrodes (Ref. 3) must be applied. For the dimensions of the NASA sensor head, this factor is 0.64. With this correction, the equation yields μ values that are higher than the nominal ones (2,000 and 200) by 15% for the small aperture and by 70% for the large aperture. The trend of these deviations conforms with the theoretical expectations, based on the details of the geometry.

5.2 SPM ELECTRONICS DESIGN

A block diagram of the SPM is shown in Figure 5-3. Sensing of the field is done using a vibrating electrode driven by a tuning fork. Directly above the sensing electrode is an aperture plate(s) containing a hole for controlled penetration of the electrostatic field created by the charge on the collector plate. As it vibrates, the sensing electrode generates a displacement current that is proportional to the net field and at the vibration frequency. The phase of this signal is determined by the polarity of the net field. The field at the sensing electrode is nulled to zero by driving the aperture plates(s) to a voltage inversely proportional to that producing the field. By proper selection of the geometry, particularly the hole size in the aperture plate(s), the electrostatic field created by the charge on the collector plate can be tailored to allow nulling the maximum field with a maximum of 10 V applied to the aperture plate(s).

Since two ranges are required, two active aperture plates are used with two hole sizes corresponding to the required attenuation for each range. An auto-range circuit makes the proper connections to control range switching. Each aperture

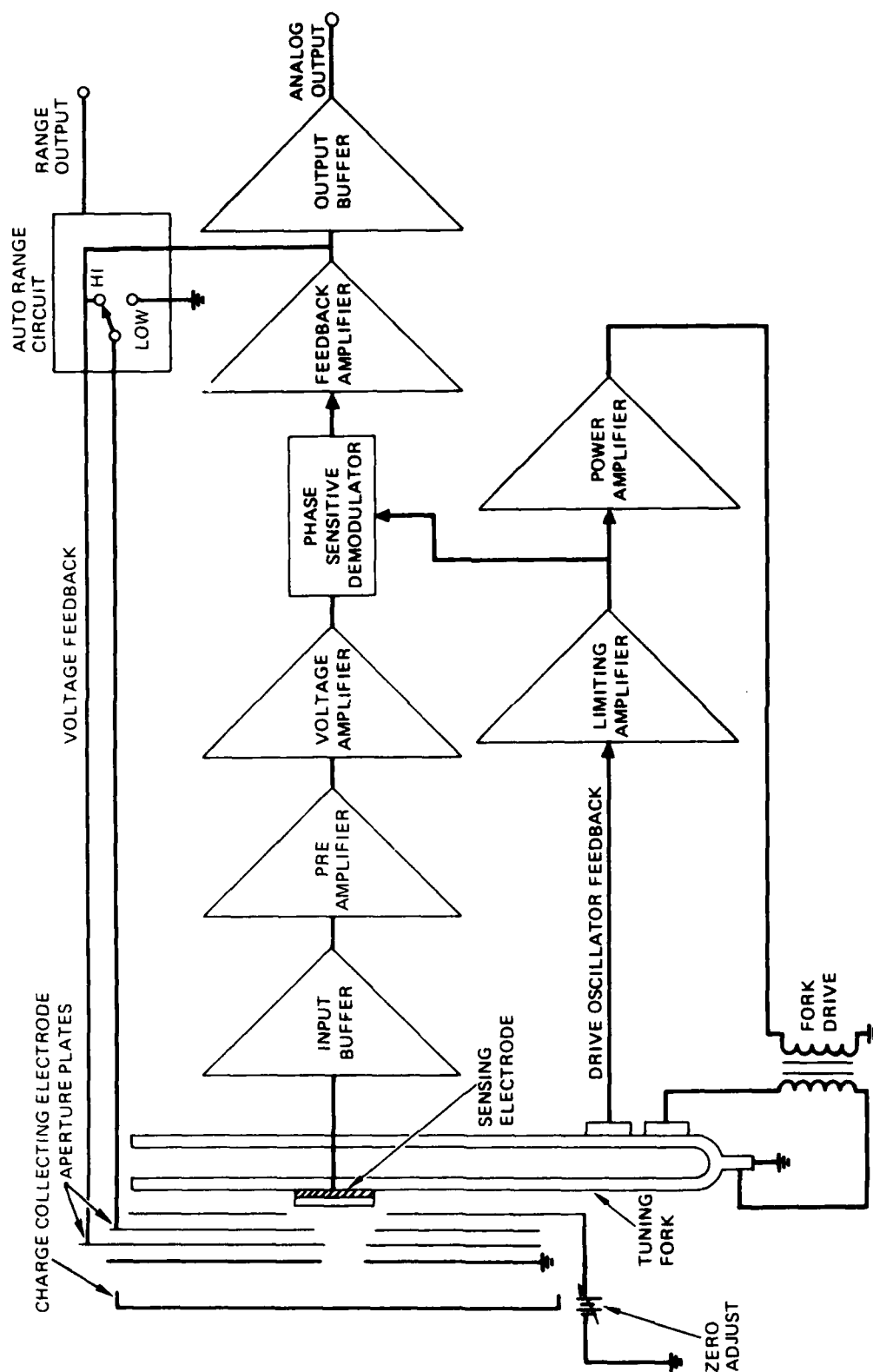


Figure 5-3. Surface potential monitor functional diagram.

plate has its corresponding aperture sized so that the low range is 200 V per volt and the high range constant is 2000 V per volt. The maximum feedback voltage then corresponds to the desired ± 2 kV and ± 20 kV of the full-scale ranges. The output of the instrument is derived directly from the ± 10 V feedback signal by attenuating it by a factor of 4 and offsetting it by 2.5 V to provide a 0- to 5-V telemetry signal.

The circuit is basically a servo-amplifier providing an output of 0 to ± 10 V which is used to drive the sensed signal to a null. In addition to the signal amplifier, a means of driving the tuning fork is required. To get the maximum amplitude of oscillation with minimum power, the fork is driven at its self-resonant frequency. This is done by deriving a feedback signal from the motion of the fork and using it to generate the drive. A pair of piezoelectric crystals are used as both the drive and feedback elements, and are mounted on the bottom tine of the fork. Piezoelectric drive, as opposed to magnetic drive, has the advantage of ease of shielding and the absence of external magnetic fields that might influence other spacecraft instruments.

THIS PAGE INTENTIONALLY LEFT BLANK

SECTION 6

TRANSIENT PULSE MONITOR (TPM)

The main criterion for the selection of the TPM sensor design is the requirement to maximize the ability to discriminate between signals generated by arcing events and signals due to "legitimate" spacecraft circuit transients. A secondary consideration is the necessity to register arcs occurring anywhere on the spacecraft surface with a minimum number of sensing elements.

A review of the literature revealed that the following types of effects are caused by arcing on a spacecraft:

- (1) The arc causes "blow-off" of a cloud of electrons which rapidly disperses. This geometrical change causes a pulse of electrostatic field which can be detected by capacitive coupling to an electrometer plate. This electrostatic field can be detected, weakly perhaps, beyond the line-of-sight.
- (2) The arc creates a plasma which radiates at high frequency. This causes a pulse of wide-band RF energy to appear, with its source in the plasma cloud and randomly polarized. This energy can be detected by antennas (horns, dipoles, monopoles, etc.) in line-of-sight only.
- (3) During the pre-arc stage, an increasing electrostatic potential appears (probably at the surface) of dielectric materials. The arc causes a substantial collapse of this potential, which can be detected by capacitive coupling to an electrometer plate. The width of the finally detected pulse is determined by the low frequency response of the detection equipment, rather than any characteristic of the arc signature itself. The collapse of the potential can be detected beyond the line-of-sight.
- (4) The arc causes displacement currents to flow in the conducting skin of the satellite, which can be detected by current sensors.
- (5) The arc causes a visible flash; it is theoretically possible to detect by line-of-sight only and probably very difficult to detect in bright sunlight.
- (6) The arc causes a release of compressive mechanical force in the dielectric and is probably impossible to use.

- (7) Acoustical vibrations are set up in the material (thunder, if the satellite were not in a vacuum). Not well documented.

Only (1), (2) and (3) were seriously considered as signals to be detected. Our design uses electrostatic-field detection, using a 123-cm² plate mounted at the outside surface of the satellite. The signal sensor is followed by a high impedance buffer with a bandwidth of about 250 Hz through 70 MHz. The buffer drives analog circuits which detect positive and negative pulses above a commandable threshold setpoint, the pulse width of signals above threshold, and the positive and negative peak amplitudes. The analog signals are converted to digital data and stored in memory under control of a small dedicated microprocessor which also contains algorithms for interpretation of the data.

With the addition of the internal sensor, the microprocessor can compare the internal and external signals to improve the rejection of transients caused by normal satellite switching events.

6.1 SELECTION OF DETECTION METHODS

We had the option of using either an rf envelope detector or a wideband amplifier as the TPM front end. The term "radiated electromagnetic noise pulses" can mean (a) "pulses of (rf) noise," or (b) "randomly occurring pulses that, taken together in their randomness, constitute noises". While our proposal adopted a design based on interpretation (a), i.e., an rf envelop detector, additional scrutiny of the implications of the two alternatives led us to favor an approach based on interpretation (b), i.e., detection of the actual signal in the frequency range of 250 Hz to 75 MHz. We are now convinced that the best overall system characteristics will result from using a single broadband amplifier with the full pulse analysis functions specified in the RFQ, connected to a single non-distributed antenna outside the spacecraft's Faraday cage, and a supplementary broadband amplifier with greatly simplified pulse analysis capabilities connected to a single non-distributed antenna inside the Faraday cage. Briefly stated, the reasons for our preference are as follows:

- (I) If only a single detector with a single antenna outside the Faraday cage is used, the ability to discriminate correctly between arcs and transients appears to be equally limited for both detection methods.
- (II) However, a single broadband antenna is more likely than a single rf antenna to pick up a detectable signal from an arcing event occurring at a location that is far below the horizon of the antenna, i.e., far from having a line-of-sight connection with it.
- (III) Regardless of the detection method, the addition of a second antenna inside the Faraday cage, in conjunction with a simple second detection circuit, offers a much increased probability of correct discrimination between arcs and transients by permitting a comparison between the signals received inside and outside of the Faraday cage.
- (IV) It is more likely for the signals received by two broadband antennas, rather than for those received by two rf antennas, that their amplitude ratios will characterize arcs and transients properly, irrespective of the location of the event relative to that of the antennas.
- (V) Additional practical points in favor of the broadband approach are: the ease of protection from destructive overloads due to arcs adjacent to the antenna, and the lower power consumption.

Statement (I) above is based on combining the information from References 4, 5, 6, 7 and 8. According to these, no clearcut characterization based on amplitudes in any fixed frequency band, at least up to a center frequency of 1 GHz, appears feasible.

Statement (II) is based on the propagation characteristics of electromagnetic waves on the surface of a spacecraft. A comparison of typical spacecraft diameters with that of Earth shows that they differ by a factor on the order of 10^6 . Thus, the propagation on the spacecraft of waves resulting from a maximum upper cutoff frequency of 100 MHz (wavelength of 3 m) for baseband detection can be expected to correspond to the

propagation of 100-Hz (3,000-km) waves on (a perfectly conducting) Earth. A typical rf center frequency would be at least a factor of 10 higher (1 GHz, corresponding to 1-kHz waves on Earth). As is well known, diffraction provides excellent ground-wave propagation on Earth for such ELF waves. However, the decay ratio for ground waves with a frequency ratio of 10 (10 kHz versus 100 kHz) is on the order of 25 dB at a distance from the origin of 1/5 of the Earth quadrant (Ref. 3). Extrapolation of the curves in Ref. 3 to a distance of 1/2 of the Earth or spacecraft circumference and to the frequencies in question yields a decay ratio on the order of 50 dB for this worst case of an arc occurring diametrically opposite the antenna.

Statement (III) is based on the observation that, regardless of the mechanism for the generation of the electromagnetic emissions, the spacecraft's (imperfect) Faraday cage will cause a significant attenuation of the signal, whether propagating inward or outward. This observation is due to Ref. 8.

Statement (IV) is based on similar considerations as (II), taking the likely blockage of line-of-sight propagation within the spacecraft's Faraday cage into account.

Statement (V) requires no further elaboration.

6.2 TPM SYSTEM DESIGN

The remote signal sensor consists of a 123-cm² plate driving a buffer amplifier (see Figure 6-1). This remote sensor and buffer is connected to the TPM electronics unit via a coax signal cable and wires for ± 12 -V power. The sensor/buffer act as a capacitive potential divider from the electrostatic field of the arc to the spacecraft frame. Two scaling input capacitors (20 pF or 640 pF) to ground are selected by a relay to provide two dynamic ranges of 10 to 300 V/m and 300 to 10,000 V/m. The input signal to the buffer has a dynamic range of ± 0.025 to ± 0.75 V. The mechanical design of the sensor is shown in Figure 6-2.

The TPM electronics unit consists of circuitry to detect positive and negative pulses above a commandable threshold set point, the pulse width of signals above threshold and the positive and negative peak amplitudes. We are not providing the

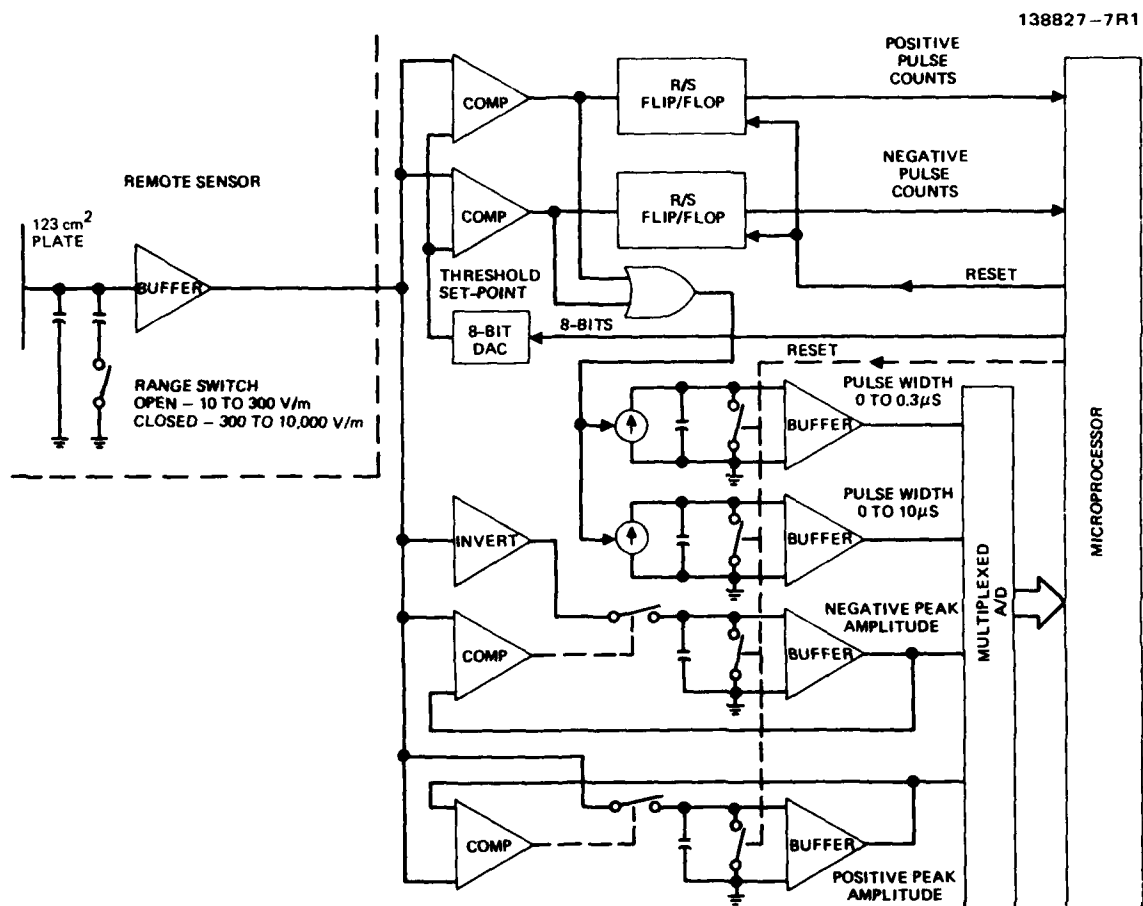


Figure 6-1. Block diagram of the TPM.

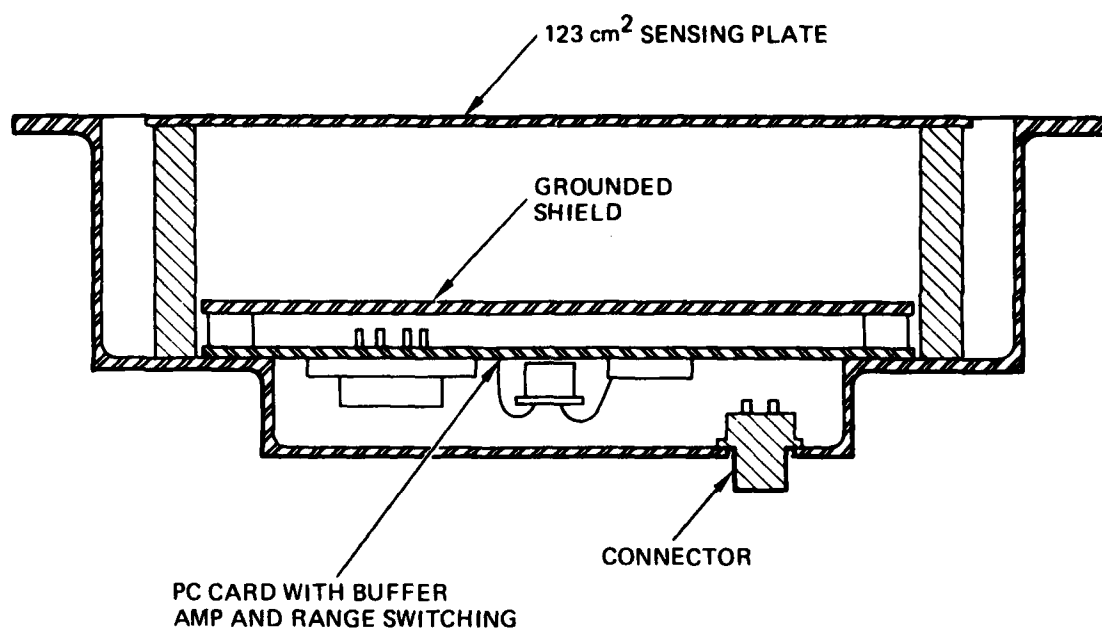


Figure 6-2. TPM sensing head design.

integrals of the positive and negative pulses since we already know their amplitude and width. D/A converters set the threshold levels, a multiplexed A/D converter is used to convert analog signals to digital, and a dedicated microprocessor controls the TPM and exercises the transient pulse algorithms for arc discrimination.

The threshold detectors are fast comparators that compare the positive and negative pulses with the commanded threshold setpoint and produce an "above-threshold" logic signal. The comparators each drive a RS latch which provides a 1-ms lockout before another pulse can be detected. The microprocessor resets the RS latch after 1-ms and also stores the pulse count in memory.

The pulse-width detectors use the "above-threshold" logic signal to gate a constant current source into a hold capacitor. The voltage on the capacitor is then proportional to the width of the pulse and is measured by the A/D and stored in memory. The capacitor is reset to zero at the end of the 1-ms lockout. Two pulse-width detectors permanently connected are used, one scaled for 0 to 0.3 μ s and the other for 0 to 10 μ s. The microprocessor looks at the 0 to 0.3- μ s range and if it is not full scale, then it uses that data. If this range is full scale, then the microprocessor takes its data from the 0 to 10- μ s range.

The peak-amplitude detectors are fast peak-voltage detectors which store the peak amplitude on a capacitor which is then measured by the A/D and stored in memory. The capacitor is reset to zero at the end of the 1-ms lockout.

The microprocessor and its interfaces consist of a radhard 80C85 with 256 words of CMOS RAM, 2K words of CMOS EAROM, 8-bit CMOS D/A converters, an 8-bit CMOS A/D with multiplexer, and a parallel interface to the system controller.

The data provided by the TPM is as follows;

Data from the external antenna:

- o No. of positive pulses above threshold
- o No. of negative pulses above threshold

- o Amplitude of the largest-amplitude positive pulse
- o Amplitude of the largest-amplitude negative pulse
- o Width of the largest-amplitude positive pulse
- o Width of the largest-amplitude negative pulse
- o Amplitude of the widest positive pulse
- o Amplitude of the widest negative pulse
- o Width of the widest positive pulse
- o Width of the widest negative pulse.

Data from the internal antenna:

- o Amplitude of the internal pulse corresponding to the largest-amplitude external positive pulse
- o Amplitude of the internal pulse corresponding to the largest-amplitude external negative pulse
- o Amplitude of the internal pulse corresponding to the widest external positive pulse
- o Amplitude of the internal pulse corresponding to the widest external negative pulse.

General data:

- o Relay status (readback of relay setting command).

SECTION 7

CONTROLLER

In this section we describe our hardware design and software architecture for the FMDS Controller. Flow charts of the major software routines and algorithms are also presented.

7.1 CONTROLLER HARDWARE DESIGN

Figure 7-1 shows the hardware architecture of the FMDS Controller. The design includes several noteworthy features which are primarily exploitations of the availability of a new family of radiation-hardened CMOS devices. These features are:

- o Dual microprocessors
- o UART serial interfaces
- o Use of EAROM.

In the discussion below, we describe these design features, and then discuss the software consequences.

The controller design employs two separate HS80C85RH microprocessors: one microprocessor ("ESA") services the ESA, producing a "vehicle potential" signal; and a second microprocessor ("master") serves the functions of operating the plasma source, maintaining command and telemetry contact with the spacecraft, and determining when to activate the plasma source (based on inputs from the TPM, ESA processor, and SPMs). This two-processor approach is desirable because the comparatively heavy total computational requirement (which is dominated by processing ESA spectra to determine the vehicle potential) makes it unlikely that a single microprocessor will be able to keep up with the 1-s sweep time of the ESA. The use of one processor for the single activity of processing ESA data is a logically desirable approach which also avoids the need for an interrupt-driven multitasking executive.

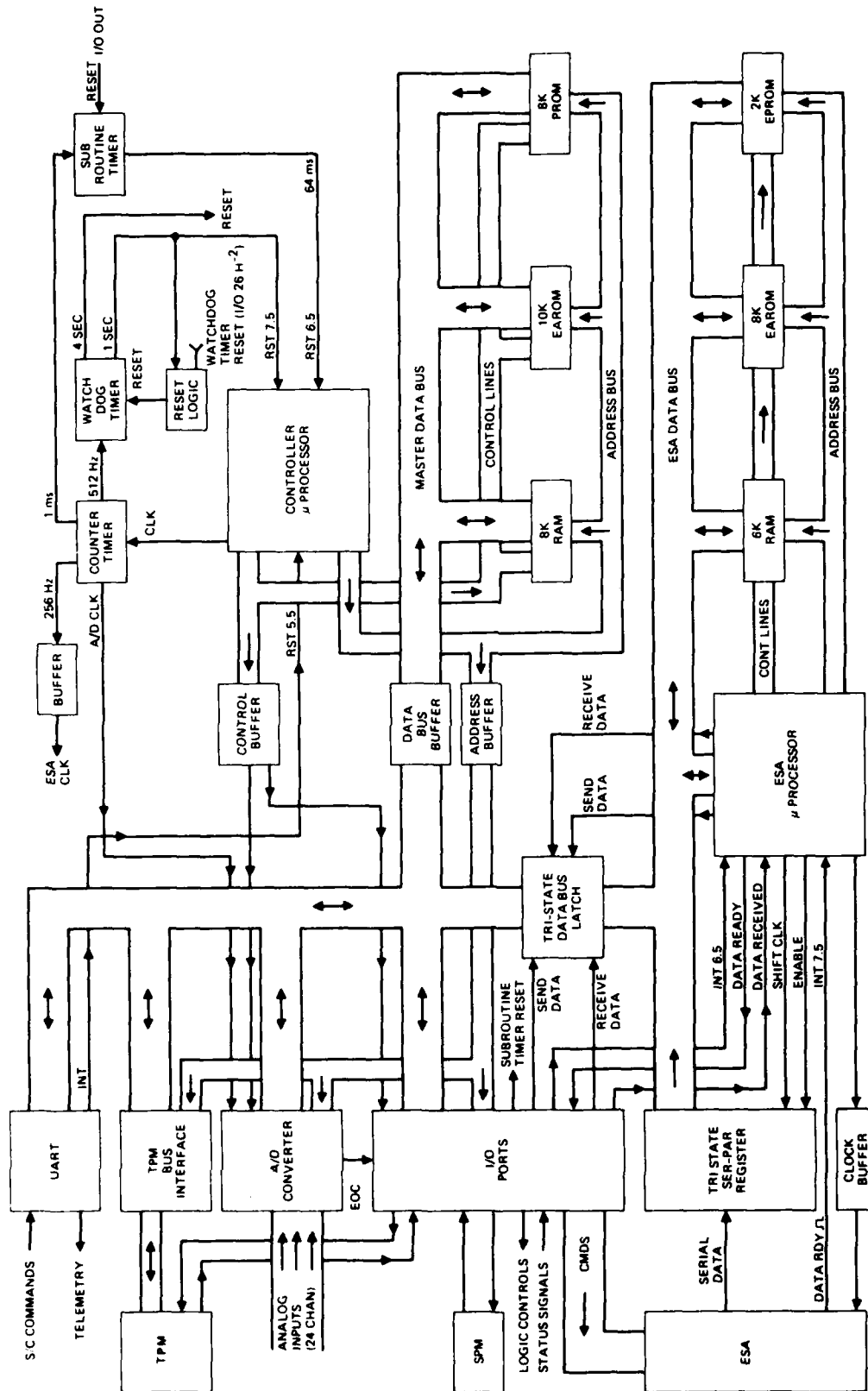


Figure 7-1. Controller hardware block diagram.

A UART (Universal Asynchronous Receiver-Transmitter) is used to perform serial communication with the spacecraft. We have chosen this approach to serial communications interface in the interest of simplicity. The UART accomplishes the work of many chips and the availability of radiation-hardened CMOS devices (Sandia SA3188, Harris HS82C56RH) may drive future spacecraft design in the direction of standard UART-based serial communications. No serial-communications standard presently exists for spacecraft, yet we must now adopt a serial communications approach which will be compatible with future spacecraft. The present UART choice increases the probability that the FMDS will be compatible with future spacecraft without modification of its serial-communications protocol.

EAROM (Electrically Alterable Read-Only Memory) is used instead of the combination of ROM and RAM that we have used in previous spaceborne systems, such as the IAPS (Hughes/NASA-LeRC Ion Auxiliary Propulsion System). In these previous systems, default set points and logic decision thresholds were contained in ROM and were copied into RAM on system powerup. The RAM values were the ones that were actually used by the system, thus permitting new values to be uploaded into RAM from the ground (via a RAM-write command). Because of the extent of this RAM and the criticality of its contents, separate error-correcting hardware was required to avoid system errors which could result from cosmic-ray-induced bitflips. Our approach for the FMDS Controller exploits the new availability of radiation-hardened CMOS EAROM (Sandia SA2999). We are housing both the FMDS operating algorithms and the default set points in EAROM. This approach has several substantial advantages: (1) the amount of RAM required is minimized; (2) the probability of bitflip-generated hazards to the system is small enough that separate error-correcting hardware is not required, and simpler measures (such as the use of byte-wide flags) provide more than adequate protection; (3) virtually all parts of the software can be rewritten from the ground, rather than

just selected set points; (4) a system reset or power outage will not cause unwanted default set points to reappear (as is the case with the IAPS controller). The Sandia EAROM device is specified for 10,000 erase/write cycles and a 10-year retention period. These are entirely adequate to FMDS objectives.

7.2 CONTROLLER SOFTWARE DESIGN

In this section we describe the software architecture design for the Controller hardware discussed above.

The software design is heavily modularized, consistent with modern design practices. An "executive" routine is present, which simply calls other modules in sequence. The advantage of this approach is that individual modules can be altered, deleted, or relocated with little or very minor alteration of the overall code. The software is realized in a machine-intimate high-level language (C), but many portions are coded in assembly language for additional speed and memory-use efficiency requirements. We have specified a high-level language because this approach is essentially self-documenting, while even well-documented assembly coding is frequently impregnable.

The overall software architecture consists of the "Executive" routine, shown in Figure 7-2, which is the controlling force of the master microprocessor. This routine is called by the 1-s interrupt (hardware implemented). Upon entering the routine, the system (microprocessor state just prior to the 1-s interrupt) is saved on the stack and the "watchdog timer" is reset. (The watchdog timer is implemented in hardware; if it is not reset at least once every four seconds, it resets the entire system.) The 1-s flag is checked and if it is set, this indicates that the microprocessor did not have time to execute all of the executive routine the last time before it was interrupted again by the 1-s interrupt. This should not normally occur and if it does an error flag is set. The 1-s flag is then set to indicate that we are in the executive routine after which all timers are decremented by

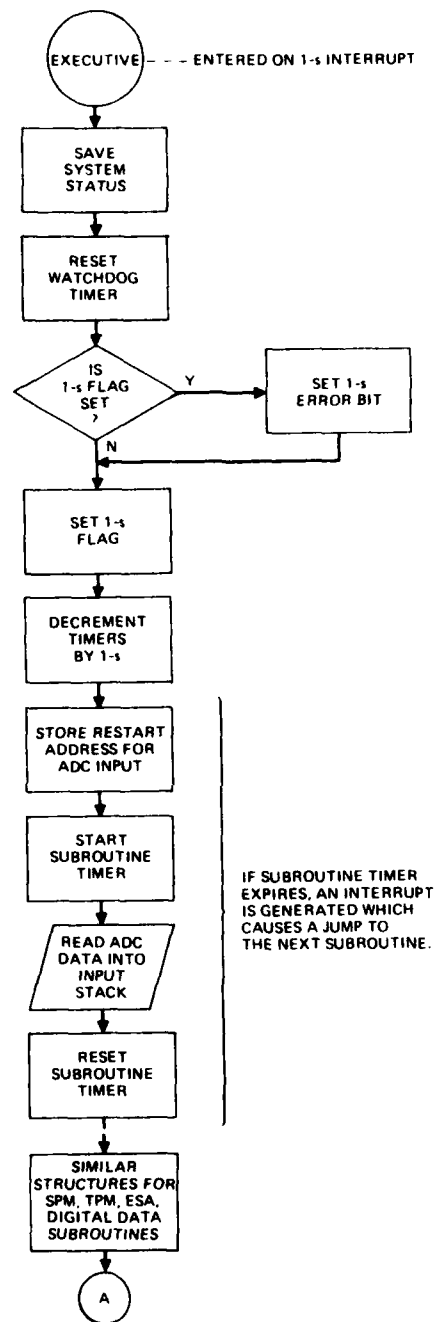


Figure 7-2. Controller executive routine.

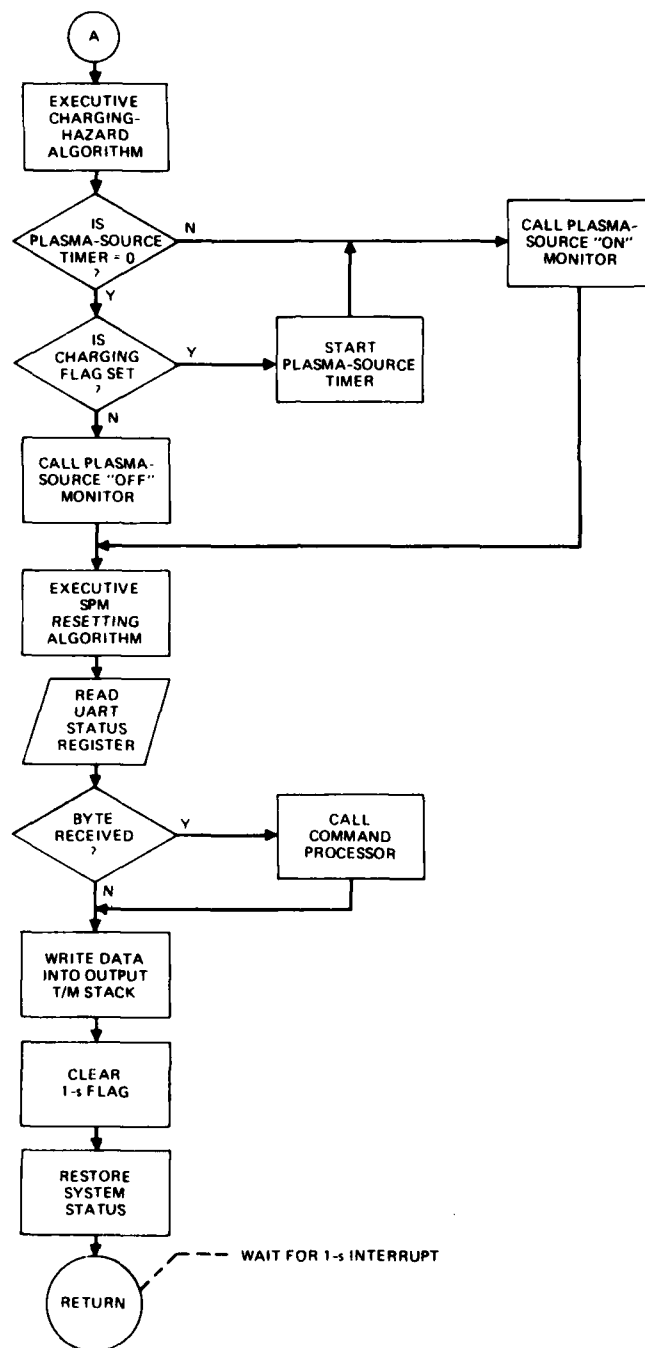


Figure 7-2. Continued.

1 s. Several subroutines are then executed to digitize the analog data, service the SPMs, TPM, and the ESAs, and to input digital data. A subroutine timer exists which generates an interrupt and causes a jump to the next subroutine if the present subroutine is not executed in a preset period of time. This prevents the microprocessor from becoming trapped in an endless loop by a malfunctioning external device (SPM, TPM, ESA microprocessor, ADC, etc.). The charging-hazard algorithm is executed next which determines whether or not the plasma source should be on. This is followed by the routine to turn the plasma source on and off and monitor its condition. The algorithm to reset the SPM input electrodes once or twice per day is executed next, followed by the routine to read the UART and input command bytes if present. Data is then written into the output telemetry stack from where it can be sent to the spacecraft (actual outputting of telemetry data to the spacecraft is handled by another interrupt driven routine). Clearing of the 1-s flag and restoring of the system status allows the microprocessor to return to what it was doing when the 1-s interrupt occurred.

The charging detection algorithm is shown in Figure 7-3. It checks the ion ESA data to see if the spacecraft potential is above the threshold level. If it is, it then checks for the sweep rate of the ESA. If the ESA is in the 16-s sweep, it requires two successive indications of charging before the charging flag is set. If the ESA is in the 8-s sweep, it requires three successive indications of charging before the charging flag is set, and if the ESA is in the 4-s or 1-s sweep, it requires five successive indications of charging before the charging flag is set. The algorithm then checks the electron ESA data and if it indicates that a charging environment is present, that the spacecraft is in eclipse (if the eclipse detection is enabled), and if the same requirements as for the ion ESA sweep time are met, then a charging flag is set. The SPMs are checked next and if at least one of them

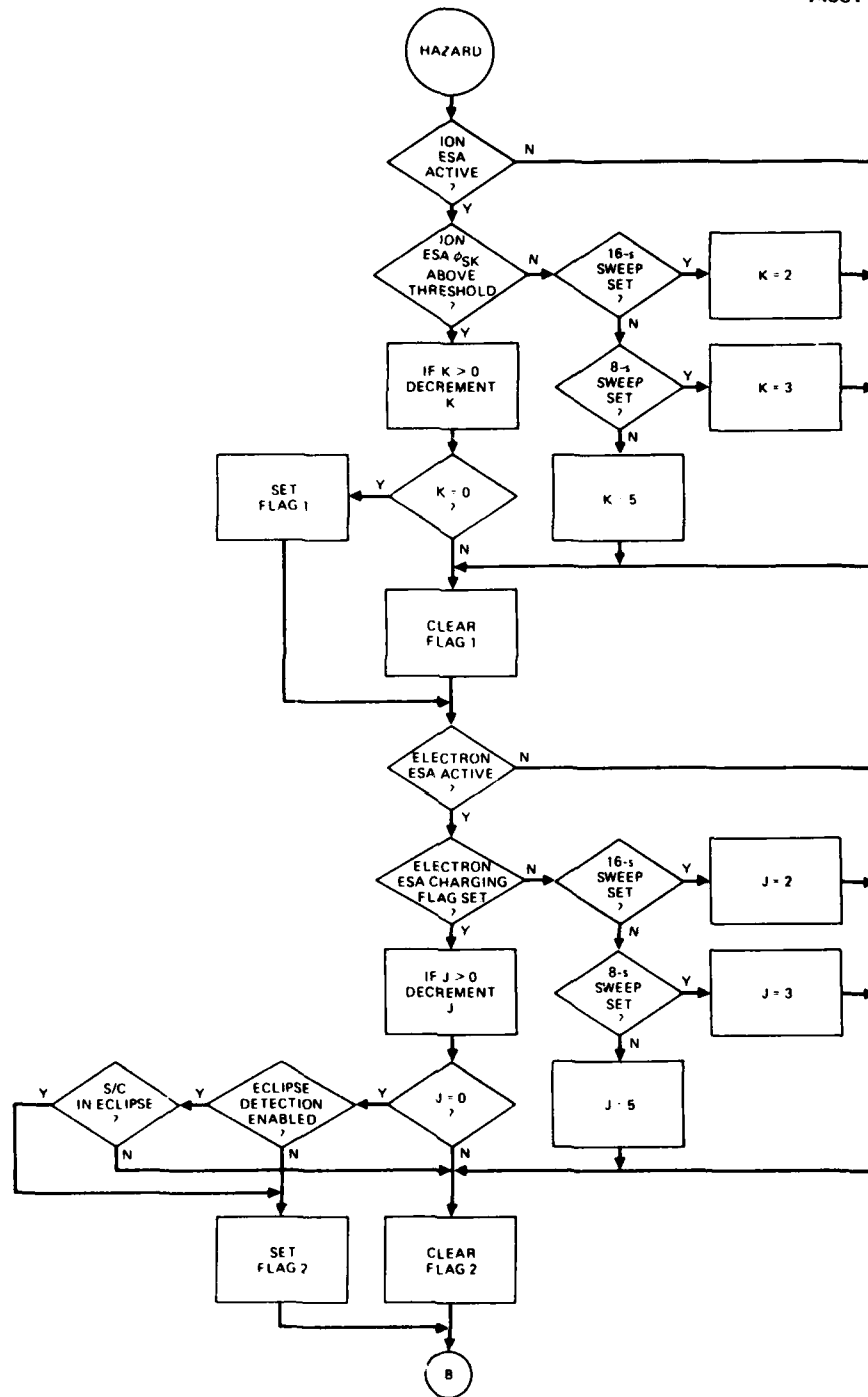


Figure 7-3. Charging detection algorithm.

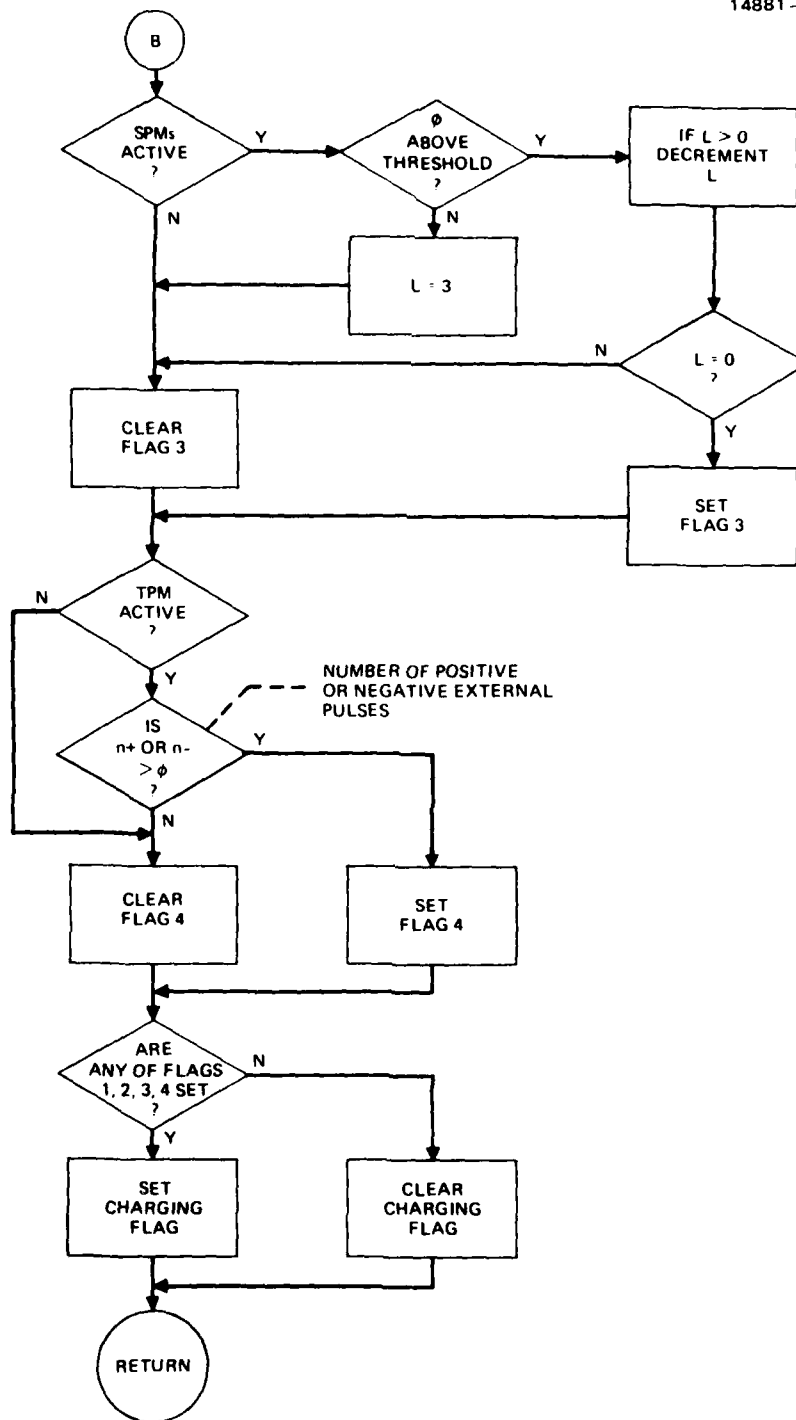


Figure 7-3. Concluded.

indicates charging above the threshold level for three seconds in succession, then a charging flag is set. The TPM is the final sensor to be checked; if it indicates that an arc has occurred, then a charging flag is set. If any charging flags are set, then the plasma source is activated.

When the requirement for charging protection has passed, the software will maintain plasma-source operation until two conditions are satisfied: (1) a preset timeout, set at the time of plasma-source ignition has expired, and (2) the charging environment has been absent for a predetermined period of time. The approach avoids excessive plasma-source reignitions during periods in which the orbital environmental conditions are fluctuating strongly.

The second, or ESA, microprocessor performs a single function: it interprets the ion and electron energy spectra generated by the ESA. The ESA microprocessor inputs data from the ESA and stores it in RAM. When a full spectrum has been input (16 channels), the processor begins execution of algorithms which determine if the net vehicle potential has exceeded a preset threshold and if a charging environment is present.

The template-matching-algorithm (TMA) shown in Figure 7-4, is our leading candidate for interpreting the ion-ESA data. It is reasonably fast, it will always return a charging potential, and it is relatively insensitive to noise effects in the spectra. It is implemented by preparing a number of "templates": dummy spectra which have been calculated to have edges and shapes corresponding to varying degrees of spacecraft charging. The TMA sequentially compares the actual ion-energy spectrum with each of the templates, which are stored in memory. The algorithm produces a vehicle potential which corresponds to the closest-match between a template and the ESA output. The algorithm uses a simple area-subtracting routine to compare spectra. This avoids the heavy computational burden associated with true correlation-coefficient calculations. We are testing this algorithm using a large number of ion-ESA data from the SC9 instrument on the SCATHA spacecraft.

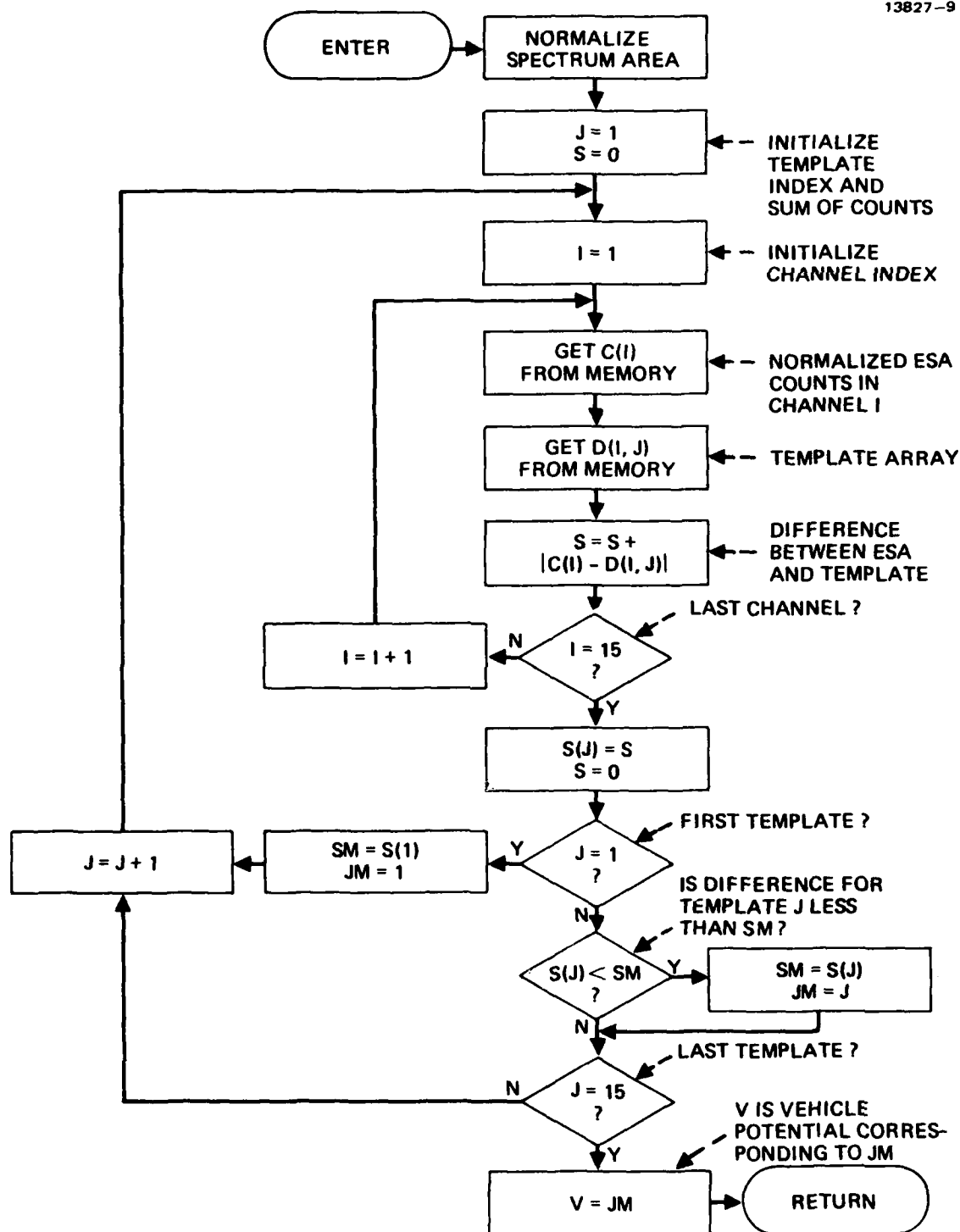


Figure 7-4. Template-matching algorithm (TMA).

We also examined the "distribution-function-algorithm" (DFA) authored by Herb Cohen of AFGL and Stanley Spiegel of the University of Lowell. This algorithm (shown in Figure 7-5) examines adjacent ESA energy channels to find an abrupt increase in ion counts from one channel to the next. The algorithm calculates the difference of counts between adjacent channels and determines whether this difference is both large enough and of adequate statistical significance. The sharp rise in count rate is assumed to result from the acceleration of ambient low-energy ions through the potential difference between the spacecraft and local space plasma. If this potential difference is V_s , then no space-potential ions can traverse the ESA when it is tuned to an energy lower than eV_s . This situation creates an ion energy spectrum which has a characteristically sharp edge below which there are (ideally) no ion counts. (Some counts are, however, found in the "impossible" region between energies of 0 and eV_s ; these counts are probably due to spacecraft-generated charges.) The DFA seeks to identify the spectral edge at energy eV_s by looking for a large and statistically significant increase in count rate between adjacent channels. This algorithm has been extensively tested (by Spiegel) using SC9 data and produces reasonable results. However, it is very computational-intensive and expected to require greater than 1 s to execute using a microprocessor without hardware multiply-divide capability.

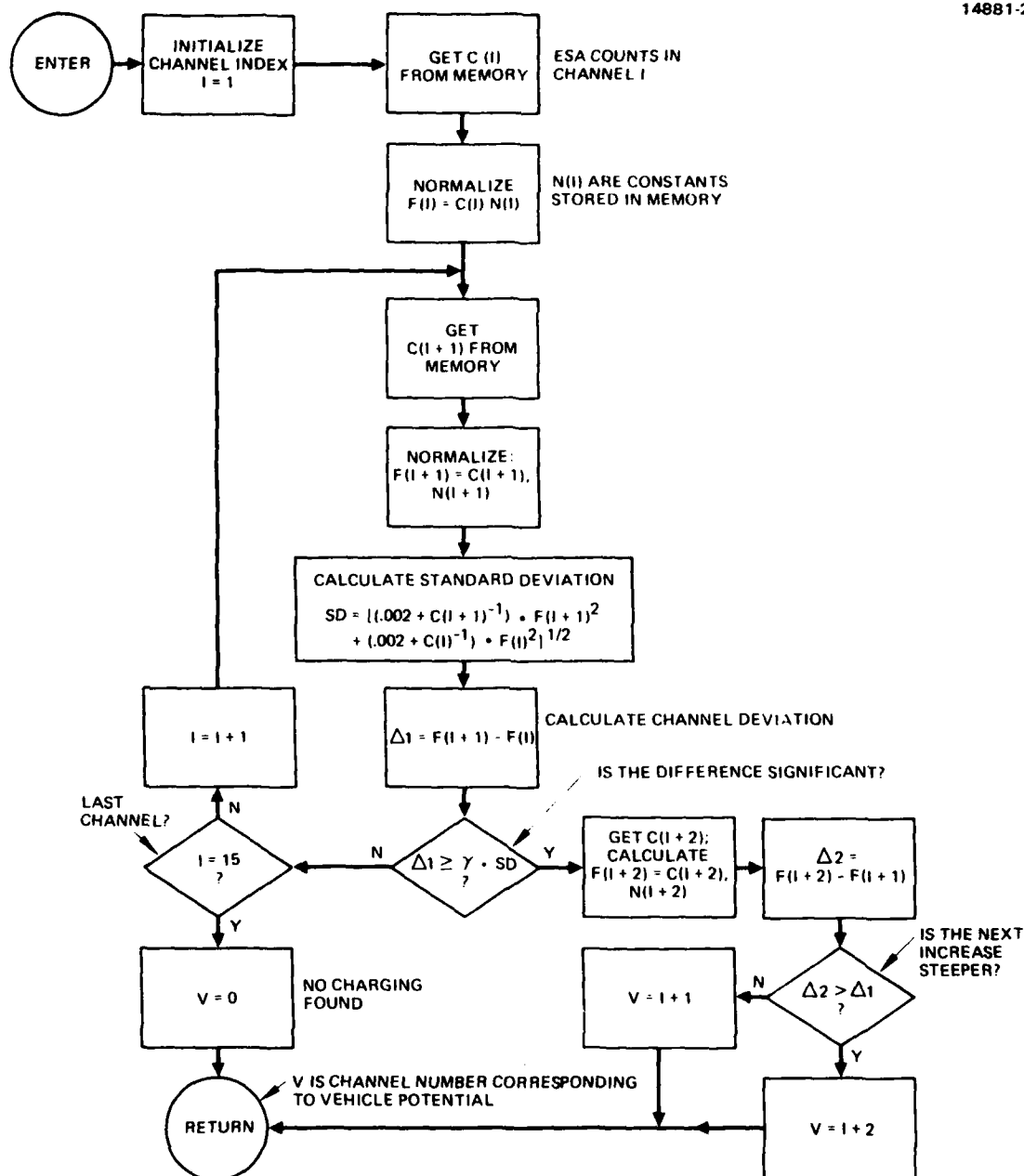


Figure 7-5. Spiegel's distribution-function algorithm (DFA).

THIS PAGE INTENTIONALLY LEFT BLANK

SECTION 8

SYSTEM DESIGN

The FMDS is designed as a self-contained system. This approach minimizes the interfaces with the satellite and makes the FMDS more attractive as a "housekeeping" function that performs the task of keeping the satellite in a neutral charge state. All electrical interfaces (command, telemetry and power) are by way of the Controller of the FMDS. This enables single types of command, telemetry, and power interfaces with the satellite. Any differences in command and/or telemetry format required by the sensors of the Plasma Source are provided by the Controller and not the satellite. All of the components of the FMDS are mounted on a flat plate, as shown earlier in Figure 2-3. This flat plate is the mechanical and thermal interface with the satellite.

The SPACECLAMP Plasma Generator for the FMDS ignites in 1 second or less; therefore, the response time of the FMDS (the time-span from the satellite reaching the threshold level selected as the critical charging level until low-energy plasma is emitted) is mainly determined by the sensor response times and the time required for the Controller to process the appropriate algorithms.

The ion Electrostatic Analyzer has sweep times of 1 s, 4 s, 8 s, and 16 s, and the algorithm associated with it may not be able to reliably detect the threshold charging level with a single sweep of data. Two to five sweeps may be necessary and therefore, if the ESA is set to the 16-s sweep, the 30-s response time is not feasible (by approximately 3 s). If the ESA is set to the 1-s, 4-s, or 8-s sweep, the 30-s response time is met (see Table 8-1). The Surface Potential Monitor responds almost immediately and its algorithm is very simple; therefore, the response time associated with this sensor is less than 4 s. The Transient Pulse Monitor also responds immediately and the

Table 8-1. Estimated Response Times of the FMDS
for the Various Charging Sensors

14881-30R1

CHARGING SENSOR	ESTIMATED RESPONSE TIME, S
ESA (1-S SWEEP)	6
ESA (4-S SWEEP)	21
ESA (8-S SWEEP)	25
ESA (16-S SWEEP)	33
SPM	< 4
TPM	< 2

algorithm to characterize the pulse and compare it to the characteristics of a surface arc is not complex. The response time associated with this sensor is less than 2 s. In general, if the ESA is swept at 8 s or less, the 30-s response time requirement is met.

8.1 ELECTRICAL DESIGN

Since the exact vehicle and/or satellite on which the FMDS will be flown is not known, the exact power, command, and telemetry interfaces are not known. Therefore, we designed for what we consider to be standard and reasonable interfaces.

The primary power return, the command return, and the telemetry return are all isolated from the case and each other by at least 1 megohm which allows the satellite to have a "single-ground-point" grounding scheme and prevents the satellite structure from being used as an intentional current carrying conductor. Our ground return isolation scheme is shown in Figure 8-1.

The design for the 28-V power-input isolation regulator is shown in Figure 8-2. This regulator provides transformer isolation between the 28-V spacecraft bus and the FMDS electronics, a 28-V coarsely regulated output to supply power to the plasma source electronics, a regulated +5-V output to supply power to the controller subsystem, multiple ± 15 -V coarsely regulated outputs for control circuits, and multiple +12-V and +15-V coarsely regulated outputs for logic circuits. Separate windings are provided for each subsystem to allow us to implement a single-point-ground system internal to the FMDS. Relays are provided to turn the power to the charging sensors and the Plasma Source on/off via commands from the Controller.

8.2. COMMANDS AND TELEMETRY

All commands and telemetry to and from the FMDS are in the form of serial digital signals. Ground isolation of digital signals is easily performed with optical isolators while ground isolation of analog signals is a much more complicated process. The use of serial digital signals (as opposed to parallel digital

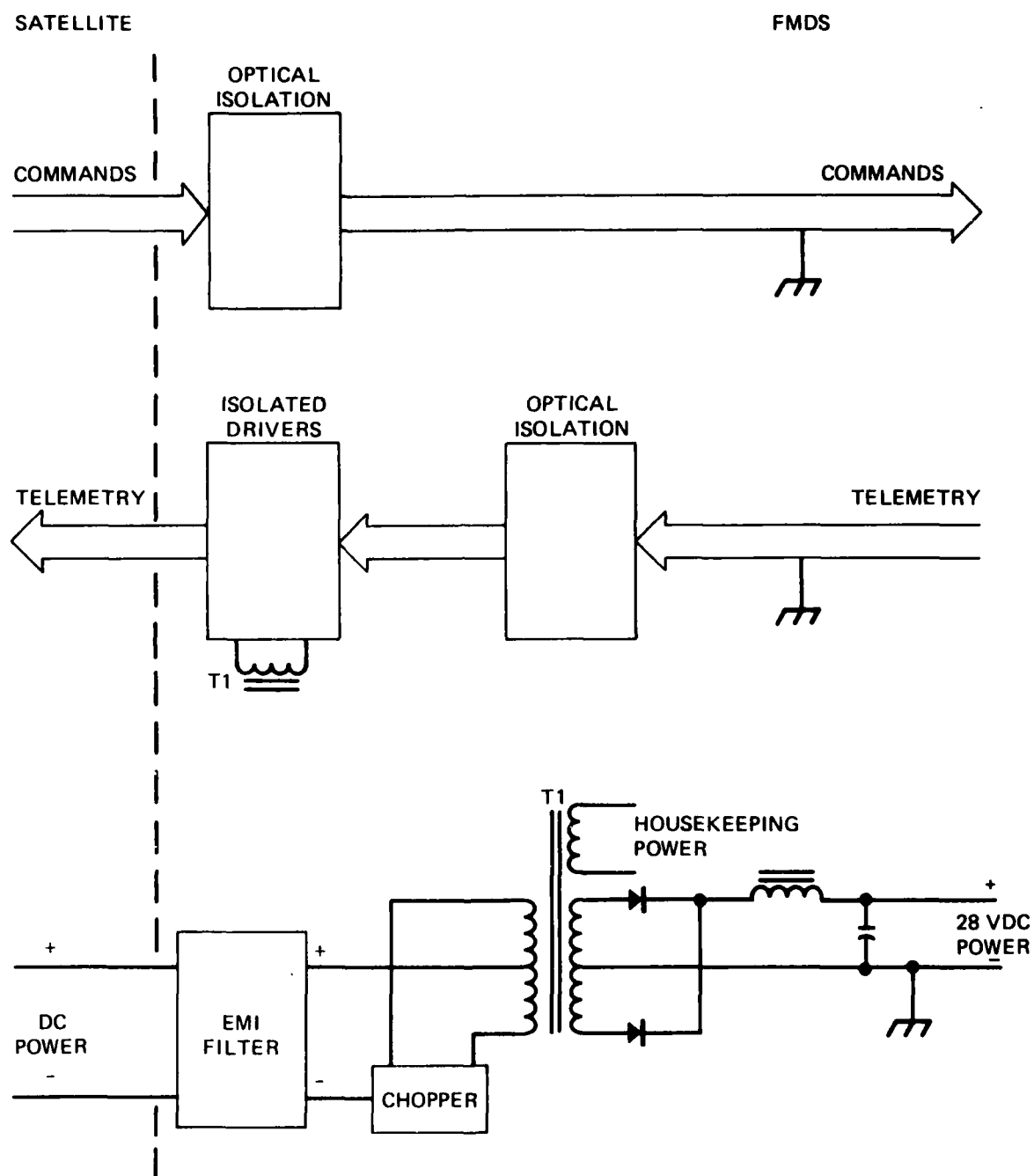


Figure 8-1. Ground return isolation.

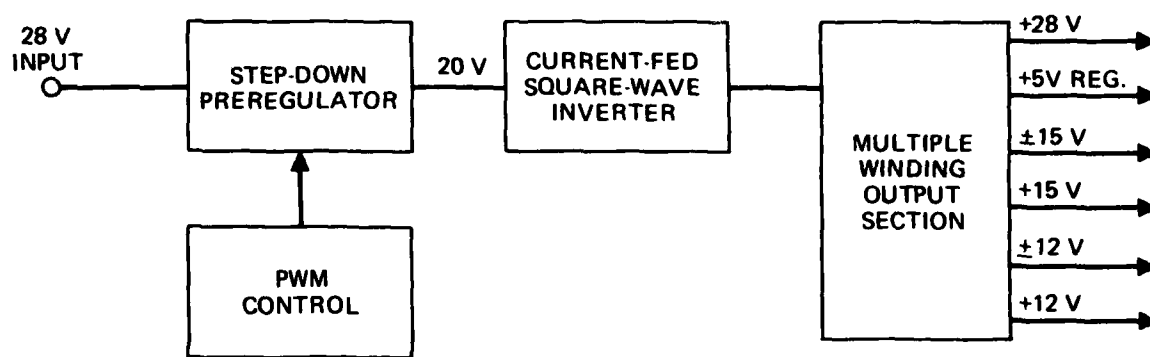


Figure 8-2. 28-V power isolation regulator block diagram.

signals) and multiplexing the commands or telemetry words sequentially over the same wires significantly simplifies the command and telemetry interfaces with the spacecraft. A typical bidirectional UART command/telemetry interface requires two data lines and two handshake lines.

Typical optical isolation and driver circuits are shown in Figure 8-3. The telemetry requires drivers that are isolated from the remainder of the FMDS and the power for these drivers is obtained from an isolated output winding of Figure 8-2.

The regulator consists of three basic sections as shown in the block diagram of Figure 8-2: (1) A pulse-width-modulated (PWM) step down preregulator which provides a constant 20-V input to the inverter section; (2) a current-fed, square-wave-inverter section which chops the 20-V power at a 40- to 50-kHz rate and provides power to (3) multiple secondary output windings.

The current-fed, push-pull, square-wave converter provides all the characteristics required of this isolation regulator:

- o Transformer isolation between input power and output power
- o Multiple output capability
- o Good cross regulation between outputs
- o Minimum complexity.

In addition, this configuration minimizes the high power stresses imposed on the switching elements during switching intervals by putting a filter choke in the input power line where it can limit the current through the transformer and the switching elements. It also prevents damage due to unbalanced dc currents and effectively turns the converter into a current source which aids in maintaining stable operation over a wide operating range. Minimum complexity is achieved by using one choke in the primary which current feeds all outputs in parallel. Since each secondary winding drives its load directly (without a choke), cross coupling between outputs is very tight, resulting in excellent cross regulation. To achieve good cross regulation, however, it is necessary to maintain a continuous, low impedance

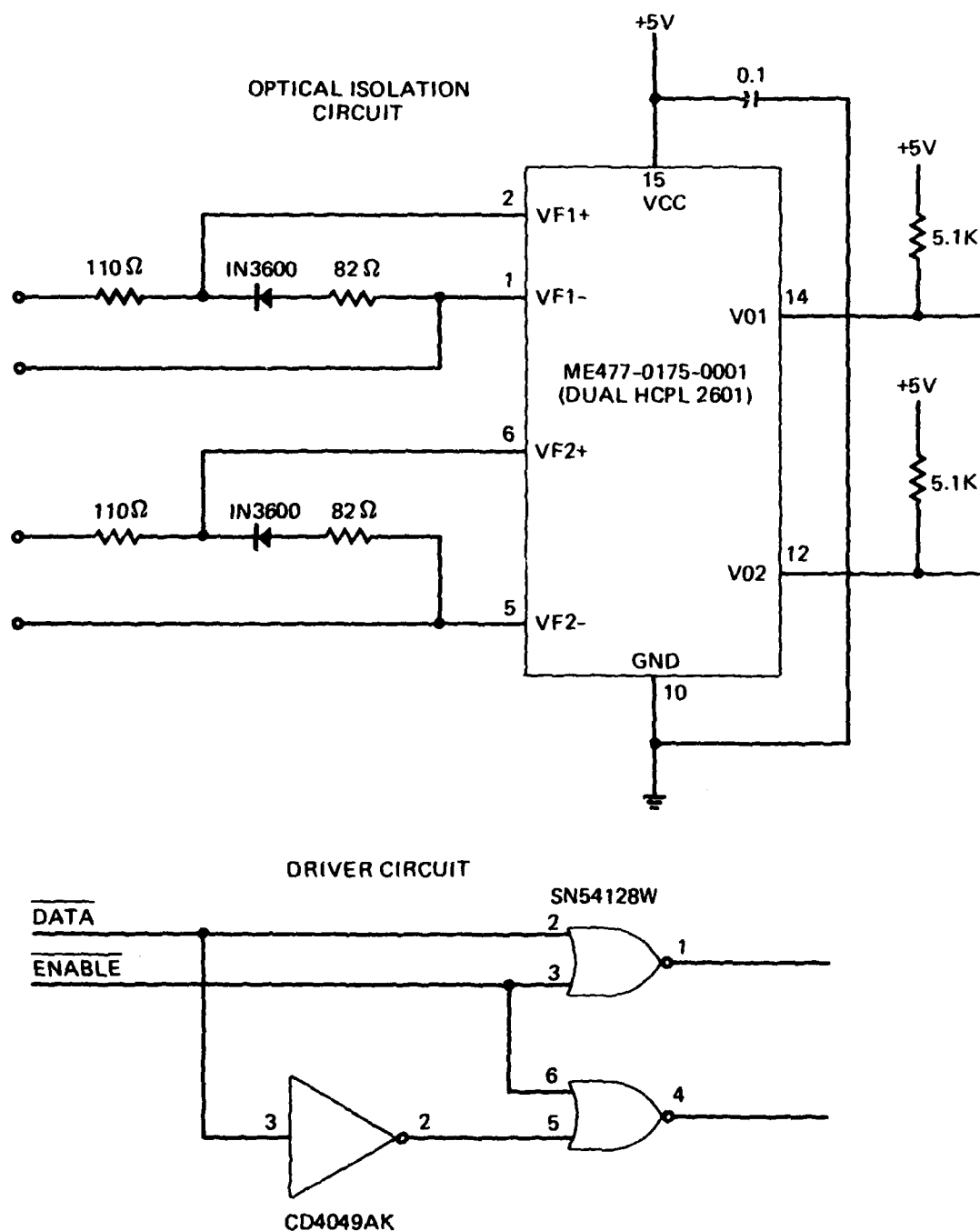


Figure 8-3. Typical optical isolation and driver circuits.

across the primary winding which dictates driving the primary winding at maximum duty cycle (50% each side) at all times. This requirement precludes using pulse-width modulation for output regulation. Instead, a Step Down converter must be used to regulate the voltage to the current fed converter, which in turn regulates all secondaries in parallel.

To minimize high frequency EMI radiation from power-distribution lines, all rectification and filtering is performed within the regulator subsystem. Only dc power is distributed to the subsystems. Ground returns internal to the FMDS are connected to its case in a manner consistent with minimizing EMI and avoiding internal ground loops. The plasma source must be referenced to the satellite frame (through the emission-current detectors to the FMDS mounting plate) for proper operation.

SECTION 9

CONCLUSION

A conceptual (breadboard) design of the Flight Model Discharge System (FMDS) has been performed. This design effort revealed no technology issues that will prevent the FMDS from achieving its ultimate goal of providing autonomous control of spacecraft charging.

THIS PAGE INTENTIONALLY LEFT BLANK

AD-A160 434

FLIGHT MODEL DISCHARGE SYSTEM(U) HUGHES RESEARCH LABS
MALIBU CA R R ROBSON ET AL. MAR 85 SCIENTIFIC-1
AFGL-TR-85-0044 F19628-83-C-0143

2/2

UNCLASSIFIED

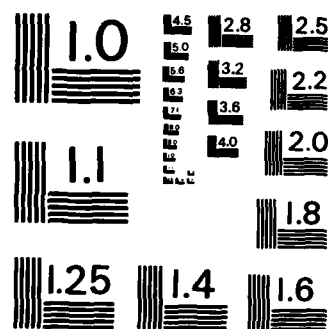
F/G 20/3

NL

END

FILED

DTIC



MICROCOPY RESOLUTION TEST CHART
NATIONAL BUREAU OF STANDARDS-1963-A

REFERENCES

1. J.C. Sturman, "Development and Design of Three Monitoring Instruments for Spacecraft Charging," NASA Technical Paper 1800, 1981.
2. K.R. Spangenberg, Vacuum Tubes (McGraw-Hill, New York, 1948).
3. H. Meinke and F.W. Gundlach, Taschenbuch der Hochfrequenz technik (Springer, Berlin, 1956).
4. P. Leung and G. Plamp, "Characteristics of RF Resulting from Dielectric Discharges," IEEE Trans. Nuclear Sci. NS-29, No. 6 (Dec. 1982).
5. P. Leung, "Discharge Characteristics of a Simulated Solar Array", unpublished paper.
6. P. Leung and P. Robinson, JPL, Pasadena, CA, personal communication, Jan. 1984.
7. JAYCOR, "Literature Review of Spacecraft Charging," Interim Contract Report, 20 October 1983.
8. M. Treadaway, JAYCOR, San Diego, CA, personal communication, Feb. 1984.

Regarding the question of what frequency spectra to expect not only from arcing events but also from spacecraft circuit transients, Dr. Treadaway stated that JAYCOR had in the past put some sensors on a TRW satellite during its qualification testing to look for signals generated by circuit transients. The result was that these signals have a non-negligible spectral content all the way up to 1 GHz. As far as spectral range is concerned, he feels that 35 to 100 MHz is most important.

END

FILMED

12-85

DTIC